American University in Cairo
AUC Knowledge Fountain

Theses and Dissertations

2-1-2019

Electroactive nanomaterials for environmental and pharmaceutical sensing

Ibrahim Hassan Abdullah

Follow this and additional works at: https://fount.aucegypt.edu/etds

Recommended Citation

APA Citation
Abdullah, I. (2019).*Electroactive nanomaterials for environmental and pharmaceutical sensing* [Master's thesis, the American University in Cairo]. AUC Knowledge Fountain.
https://fount.aucegypt.edu/etds/743

MLA Citation
Abdullah, Ibrahim Hassan. *Electroactive nanomaterials for environmental and pharmaceutical sensing*. 2019. American University in Cairo, Master's thesis. *AUC Knowledge Fountain*.
https://fount.aucegypt.edu/etds/743

This Thesis is brought to you for free and open access by AUC Knowledge Fountain. It has been accepted for inclusion in Theses and Dissertations by an authorized administrator of AUC Knowledge Fountain. For more information, please contact mark.muehlhaeusler@aucegypt.edu.

The American University in Cairo

The Graduate School

The Nanotechnology Program

Electroactive Nanomaterials for Environmental and Pharmaceutical Sensing

A Thesis in Nanotechnology

By

Ibrahim Hassan Abdullah

Submitted in Partial Fulfilment of the Requirements for

The Degree of Masters of Science in Nanotechnology

©2018 Ibrahim Hassan Abdullah

December 30th,2018

Abstract

Sensing is an important emerging technology in the current industrial era. It covers a plethora of applications from medical personalized devices to aerospace oxygen level detectors. Of those applications, environmental and pharmaceutical sensors are significantly important. Specifically, electrochemical sensors are easy to use and develop besides being cost-effective and accurate. The work in this thesis concerns the development of two sensing platforms for the detection of Hg(II) as a water pollutant, and the detection of Lornoxicam (LOR) as a pharmaceutical compound. The materials fabricated were morphologically, structurally, and electrochemically characterized. They were also tested against their analytical targets in spiked and real sample media to ensure their utility, sensitivity and accuracy. The testing results were either in the sub-nano or the pico-molar levels, with high linear range. The materials were also examined to target the analyte species in separate and co-formulated media to assure their selectivity. Furthermore, the sensing platforms were repeatedly used to test their stability and reproducibility. Titania nanotubes/reduced graphene oxide (TNTs/RGO) showed an efficient sensibility of Hg(II) in the presence of Cu(II) and Mn(II) species with no significant interference for a wide range of concentrations. On the other hand, $BaNb_2O_6$ nanofibers showed an enhanced activity towards the electrocatalytic oxidation of Lornoxicam (LOR) and paracetamol (PAR), producing remarkably high oxidation currents. Wide linear dynamic ranges, high sensitivity, very low LOD, good reproducibility and repeatability, and high stability, together with simple procedures for surface modification and determination are the advantages of the prepared sensors.

Dedication

This thesis is dedicated to my parents.

Table of Contents

List of Figures

List of Schemes

List of Tables

List of Acronyms

B-R buffer.	Britton-Robinson buffer
CNT.	Carbon nanotube
CPE.	Carbon paste electrode
CV.	Cyclic voltammetry
DVP.	Differential pulse voltammetry
EDX.	Energy dispersive X-ray spectroscopy
FESEM.	Field emission scanning electron microscopy
FTIR.	Fourier transform infrared spectroscopy
FWHM.	Full width at half maximum
GCE.	Glassy carbon electrodes
GO.	Graphine oxide
Gr.	Graphene
HMDE.	Hanging mercury drop electrode
HPLC.	High pressure liquid chromatography
HRTEM.	High resolution transmission electron microscopy
ICP-AES.	Inductive coupled plasma atomic emission spectrometry
LOD.	Limit of detection
LOQ.	Limit of quantification
LOR.	Lornoxicam
NSAID.	Non-steroidal anti-inflammatory drug
PAR.	Paracetamol
PPCP.	Pharmaceuticals and personal care products
QCM.	Quartz crystal microbalance
RGO.	Reduced graphene oxide
SEM.	Scannig electron microscopy
SPE.	Screen printed electrodes
SWASV.	Square wave anodic stripping voltammetry
SWV.	Square wave voltammetry
TNT.	Titania nanotubes
U.S. EPA.	United States Environmental Protection Agency
UPLC-MS/MS.	Ultraperformance liquid chromatography-mass spectrometry
WHO.	World's Health Organization

Acknowledgment

I thank Allah. He was always by my side. I felt his presence all along the way. This is more profound than how words can express. I am grateful for how He gave me the chance to meet many people without whom I would have never been writing these lines. In this regard, I would like to thank Prof. Nageh Allam for how he taught me a lot on both the professional and personal levels. I would like to thank Prof. Adham Ramadan and Prof. Hassan El-Fawal for their sincere and continuous support. I am grateful for every professor and staff member at AUC who helped me throughout this journey. Now I am so reminded of Ms. Aya Morsi and Ms. Shaimaa Abdel Aziz. Thank you!

I cannot forget to thank Al-Ghurair Foundation for the financial support. It was my honor to be awarded their STEM scholarship. I would like to thank my fellow members of EML who showed up for me whenever I needed help. I am grateful to the help of Dr. Mona Ali for she taught me the very basics of this thesis work. Indeed, there are so many behind-the-scenes without whom I would have never had the strength to move on. I will keep their names unmentioned for now.

Chapter 1

Introduction and Scope of The Thesis

1.1 Global Sensor Market

The personalized lifestyle of everything starting from medicine and electronics to environmental and food quality control has been a characteristic of the modern era. Sensors are a way to express this personalization such as mobile, integrated, and wearable sensors which are getting to become a commonplace. Although they now are mainly attached to physical parameters (such as pressure and temperature), sensors are soon to be personalized for many other parameters.[1] Market study of sensors is evident that more money will be invested in sensors industry as they have a real chance of progress during the following decades. For instance, the compound annual growth rate (CAGR) of sensors industry is accelerating by rate of 8%, with an incremental growth of $17.04 bn between 2017 and 2022, as shown in Figure 1-1.[2]

Figure 1-2: CAGR of sensors industry between 2017 and 2022.[2]

As nanomaterials are getting involved in sensors industry, it is attracting more attention on both the financial and scientific communities. This is due to the tremendous enhancement of sensing properties that nanostructures may grant to the

detection platform.[3] As a result, and according to Research Nester, the CAGR of chemical sensors and biosensors is accelerating by rate of 11.5%, which is even higher than that of flow and level sensors that currently sell higher in the global sensor market (see Figure 1-2).[4]

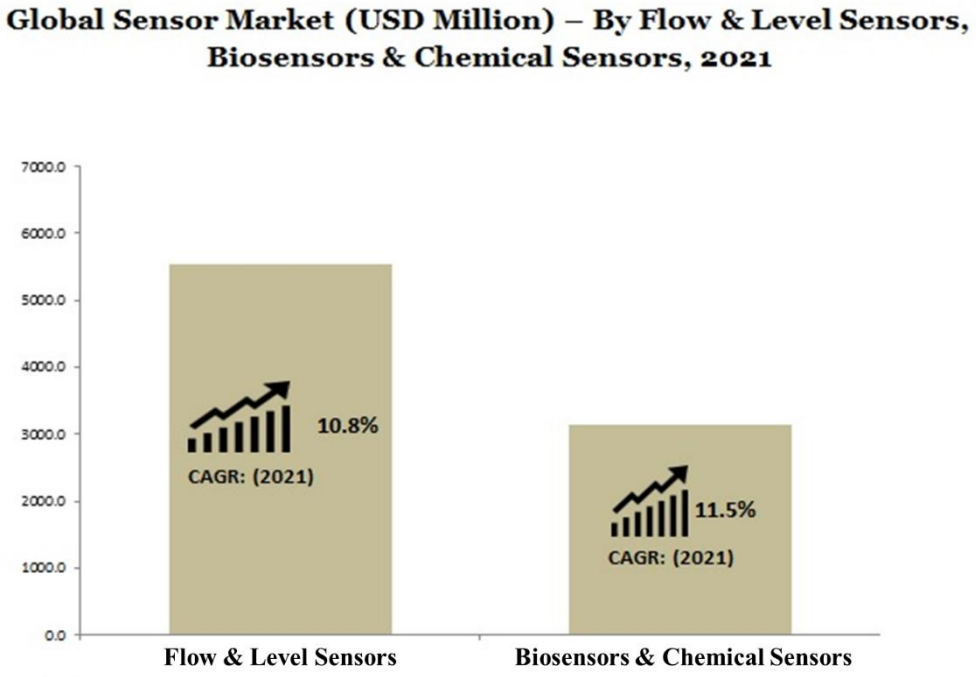

Figure 1-3: Comparison between flow & level sensors vs biosensors & chemical sensors in the global sensor market.[4]

1.2 What Are Sensors?

Sensors are devices that utilize an active and detective material toward certain analyte/s and a transducer to transfer and maybe magnify the produced signal. This signal can take different forms such as electrical, optical, thermal, or electrochemical. Such devices are used for direct determination of the targeted analyte in its sampling matrix.[5] Many methods are proposed to classify the developed sensors, one of which is according to the type of the signal previously mentioned. According to Chen and Chzo, sensors can also be classified as sensors and biosensors, depending on their

active recognizing material on the electrode. Selecting this material differs with respect to the nature of the target analyte and the kind of effective reaction between them both.[6]

1.3 Electrochemical Sensors

Electrochemical sensing is the oldest form of all chemical sensors, since the pH glassy electrodes invention by Max Cremer in 1906. After L. Clark introduced the glucose enzyme amperometric electrode, electrochemical sensors started to be common in labs chemical industries, and many other fields.[7] The feasibility of developing their recognition ability makes electrochemical sensors a good candidate for application in many disciplines such as food, biomedical, environmental, agricultural, and industrial fields. That is owing to their precise, cost effective, fast, and reliable detection of many organic and inorganic compounds.[8] However, for these sensors to continue their progress, they need multidiscipline ray research in the fields of material science, electronics, and computer science to meet the emergent needs in different fields.[9]

1.4 Objectives and Scope of Thesis

Modification of electrochemical electrodes such as carbon paste electrodes (CPEs) is an effective way to produce a better sensitive and selective detection platform for different inorganic and organic analytes. Such platforms can be used for various applications. Out of these applications, environmental and pharmaceutical ones are of considerable importance. This thesis includes development of two modifiers for the purpose of increasing the sensitivity of CPEs. The first modifiers aim to sensitive detection of Hg(II) ions (as an environmental pollutant) in presence of Cu(II) and Mn(II). The second does to lornoxicam (LOR) (as an anti-inflammatory

drug example) in a coformulation with paracetamol. This thesis will be arranged as following:

Chapter 2: Shows a concise background about the electrochemical sensing concept and its importance in the environmental and pharmaceutical fields.

Chapter 3: Presents a literature review of the recent studies in the field of electroanalytical detection of heavy metals and drugs.

Chapter 4: Designates the experimental conditions and procedures followed for the processes of electrode modification for both purposes (Hg(II) and LOR detections).

Chapter 5: Discusses the main contribution of the thesis work and shows the difference in sensitivities that this modification has aimed to achieve from electrochemical point of view

Chapter 6: Provides conclusion and future work.

1.5 References

(1) Tiwari, A.; Turner, A. P. F. *Biosensors Nanotechnology*.

(2) Global Industrial Sensors Market 2018-2022 | Rise in Demand for Smart Factories to Promote Growth | Technavio | Business Wire https://www.businesswire.com/news/home/20180918006031/en/Global-Industrial-Sensors-Market-2018-2022-Rise-Demand (accessed Dec 23, 2018).

(3) Álvarez-Romero, G. A.; Alarcon-Angeles, G.; Merkoçi, A. Graphene: Insights of Its Application in Electrochemical Biosensors for Environmental Monitoring. In *Biosensors Nanotechnology*; John Wiley & Sons, Inc.: Hoboken, NJ, USA, 2014; pp 111–140.

(4) Global Sensor Market Size : Global Industry Demand, Growth, share & Forecast 2021 https://www.researchnester.com/reports/global-sensor-market-analysis-opportunity-outlook-2021/137 (accessed Dec 23, 2018).

(5) Bagheri, S. Nanocomposites in Electrochemical Sensors.

(6) Chen, S.-M.; Chzo, W.-Y. Simultaneous Voltammetric Detection of Dopamine and Ascorbic Acid Using Didodecyldimethylammonium Bromide (DDAB) Film-Modified Electrodes. *J. Electroanal. Chem.* **2006**, *587* (2), 226–234.

(7) Cui, F.; Zhang, X. Electrochemical Sensor for Epinephrine Based on a Glassy Carbon Electrode Modified with Graphene/Gold Nanocomposites. *J. Electroanal. Chem.* **2012**, *669*, 35–41.

(8) Švancara, I.; Kalcher, K. Introduction to Electroanalysis of Environmental Samples; 2014; pp 3–21.

(9) Zhu, C.; Yang, G.; Li, H.; Du, D.; Lin, Y. Electrochemical Sensors and Biosensors Based on Nanomaterials and Nanostructures. *Anal. Chem.* **2015**, *87* (1), 230–249.

Chapter 2

Scientific Background

2.1 The Concept of Sensing

The concept of sensing varies according to the detection essay (such as chemical, optical, and immunoassay) and the type of the targeted analyte. Nevertheless, there are several general mutual principles that need to be satisfied in most of these assays. They can be concisely stated as follows:

a- Selective bonding type between the targeted analyte and the recognition platform.

b- Chemical, physical, or biological interaction at the interface between the receptor and the analyte, which should result in a characteristic signal.

c- Receiving this signal by a transducer, and then converting it into an electrical form of signals.

d- Magnifying the transduced signal by using of an amplifying detector.

e- Delivering the amplified signal to a computer for processing, quantifying, and correlating to the concentration of the analyte.[1]

2.1.1 Conventional Techniques of Analytical Detection

As there is always a demand for continuous detection of concentration for species such as drugs and heavy metals, many analytical techniques are being already used. For example, to monitor heavy metal ions concentration in their solution media, atomic absorption spectrophotometry (AAS) is almost the standard method for this purpose. The working principle depends on the thermal ionization of the metal, whose concentration is then detected by a spectrophotometer. According to the method of

sample introduction, there are two types for AAS, graphite furnace atomic absorption spectrophotometry (GFAAS) and flame atomic absorption spectrophotometry (FAAS). They both show a tolerable sensitivity; however, they are sample-destructive techniques and suffer from interference at low concentration, in addition to their time-consuming sample measurements.[2]

Another common analytical technique is atomic fluorescence spectrometry (AFS), which is a sort of atomic spectrometric methods. Nevertheless, it is based on the principle of vaporized metal atoms deactivation by means of subsequent radiation. Then, detecting the produced fluorescence, qualitative and quantitative analyses of the target species can be attained. Relatively, AFS is simpler than AAS, but still, it suffers from interference and quenching of the resultant interference.[3]

Also, inductively coupled plasma spectrometry (ICP) is another analysis technique which is built on the principle of detecting the emission of the target species instead of their absorption. As compared to AFS and AAS, ICP provides enhanced measuring process thanks to its strong emission that is based on the powerful thermal atomization. Though, the ICP system instability decreases its precision, which is a result of the unstable transfer of energy between the sample and the source of plasma in the device. This leads to the production of a hesitated ion signal.[4]

On the other hand, several analytical techniques are common for the aim of pharmaceutical detection such as high-performance liquid chromatography (HPLC),[5–7] spectrofluorimetric,[8] chemiluminescence,[9] and spectrophotometric[10] analyses. Despite the satisfactory sensitivity achieved by these techniques for pharmaceutical drugs, they frequently suffer from shortcomings such as tedious extraction procedures

from complex formulations, high cost, time consumption, and need for professional personnel, hindering the routine analyses.[11]

2.1.2 Electrochemical Sensing

Electrochemical detection techniques offer an alternative to the conventional analysis methods that are currently utilized for molecular monitoring purposes. Electrochemical determination essays mainly involve an electron transfer process across the interface between the target species and the surface of the electrode. Such assays are versatile, cost-effective, and use reagent-less sample preparation, making it less tedious. In the same manner, electrochemical analyses are non-destructive and consume very minute amounts of the sample, with low chances of contamination. This all adds to the fast, sensitive, and selective experimental results of the detection process. Consequently, electrochemical detection is promising to be automated and miniaturized for *in-situ* analysis purposes.[12]

Voltammetry, out of various electrochemical techniques used for the process of pharmaceutical and environmental detection, is the most versatile and commonly used one. This is owing to the low signal to noise ratio and the capability of simultaneous detection of different targeted elements. Typically, voltammetry is usually a three-electrode technique, involving working electrode (WE), counter electrode (CE), and reference electrode (RE) which work to produce a potential-current-time interrelated data. Figure 2-1 shows a schematic illustration of the electrochemical setup that is used for detection, recording both potential and current. The position of the peak in the graph produced from such a process is element-specific, sort of a fingerprint, whereas its magnitude is proportional to the concentration of that element.[13]

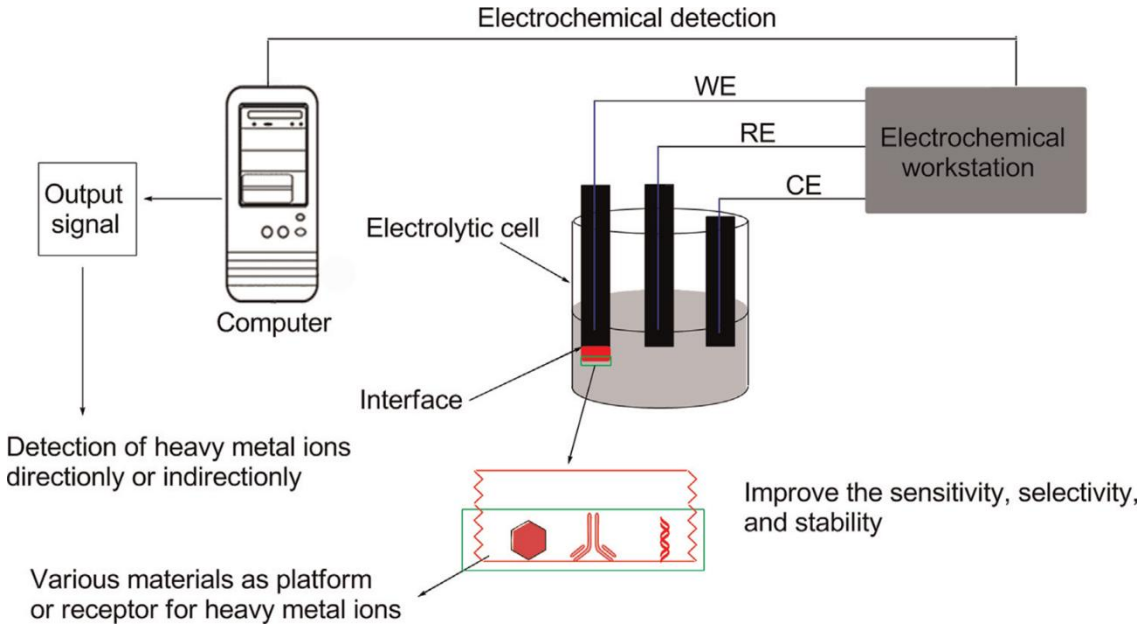

Figure 2-1: Schematic illustration of the principles of electroanalytical detection. Heavy metals are taken as an example.[14]

Voltammetry can be further enhanced by using of anodic stripping step. This could lower the detection limit down to sub-nanogram level. Generally, taking a metal ion (M) as an example, anodic stripping voltammetry (ASV) is composed of two main steps:

1- A preconcentration step, in which the targeted species accumulate on the surface of the WE in a reduction process to gain electron, attracted by the negative potential applied. This reaction can be written as:

$$M^{n+} + ne^{-} \rightarrow M^{0} \qquad (2.1)$$

Such migration from the ions toward the electrode's surface can illustrate the distinctive electrochemical sensitivity.

2- A step of voltage scanning on the surface of the WE. This leads to oxidation (stripping) of the accumulated ions back to their molecular form

in the solution at a certain potential value. This stripping causes the targeted species to convert into cations, upon collecting their electrons in a manner that is correlated to their concentration. This reaction can be written as:

$$M^0 - ne^- \rightarrow M^{n+} \qquad (2.2)$$

A schematic diagram of the whole process is provided in Figure 2-2. It is worthening that this whole process can also happen in a reversed way, which is known as cathodic stripping voltammetry.[15]

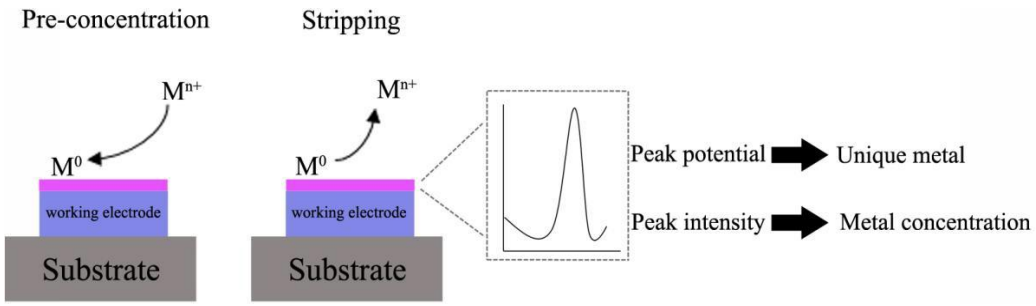

Figure 2-2: Schematic illustration of the concept of anodic stripping voltammetry (ASV).[15]

In a different manner, regardless of the numerous merits of ASV, using only bulk interfaces as electrode surfaces, still, does not meet the required accuracy for the detection process of many analytes. In case of utilizing bulk structures for electrode surfaces, several issues can raise such as:

I. High overpotential during the preconcentration step.
II. Large potential needed for the stripping step.
III. High chances of interference with the electrolyte contaminant ions of during deposition potentials.
IV. High possibility of interference with the other competitive ions in the sample.

These reasons raise the demand for surface modification of the WE to attain enhanced selectivity and sensitivity. Consequently, nanostructures have been thoroughly studied to be utilized as electrode surface modifiers.[16]

2.1.3 Nanostructured Electrode Modifiers

The last two decades have witnessed the major trend of using nanotechnology in different disciplines in which they proved their reliability and excellence. This can be attributed to their unusual properties, as they differ from bulk-structured materials in two main characteristics:

1. They are not governed by the rules of classical physics, but rather quantum chemistry.
2. They possess an enormous surface-area-to-volume ratio, which empowers a massive amount of reactant species to get into contact with electrode surface.

Consequently, a superior mass transport efficiency, signal-to-noise ratio, and high charge transfer rate were noticed using of nanostructured materials. Also, they showed relatively higher absorption capacity and lower solution resistance than those of bulk-structured materials. So, selecting the right nanomaterial as an electrode modifier, keeping in mind their above-mentioned exceptional properties, would demonstrate extraordinary selectivity and sensitivity. This selectivity would, of course, lead to utilizing electrochemical sensing in complex aqueous and biological analyte matrices such as in urine, saliva, sweat, tears, and plasma.[17,18]

2.1.4 Square Wave Voltammetry

Square wave voltammetry (SWV) is a type of pulse voltammetry which aims mainly to measure lower detection limits than normal voltammetry. Pulse

voltammetry was mainly introduced by Barker and Jenkin. The concept depends on increasing the current difference between both the faradaic and non-faradaic currents produced during the analyte oxidation on the electrode surface.[19] SWV is a differential technique of large amplitude in which a waveform is operated on the WE. This wave is comprised of an identical square wave, which is superimposed on a staircase potential (Figure 2-3 a).[20] Sampling the current takes place twice during the cycle, firstly exactly before the forward pulse ends (t_1), and secondly right before the reverse pulse does(t_2).

The products of the forward reaction undergo the reverse reaction as a result of the very large modulation amplitude of the square wave. Accordingly, the peak-current produced is almost identical around the half-potential and a function of the analyte concentration.[21] The superior sensitivity of SWV technique is a result of the fact that the net current is the difference between both the forward and the reverse ones, causing its peak to be higher than theirs (Figure 2-3 b). For both reversible and irreversible cases, SWV has proved to be 4 and 3.3 times higher than the corresponding differential pulse voltammetry measurements.[22]

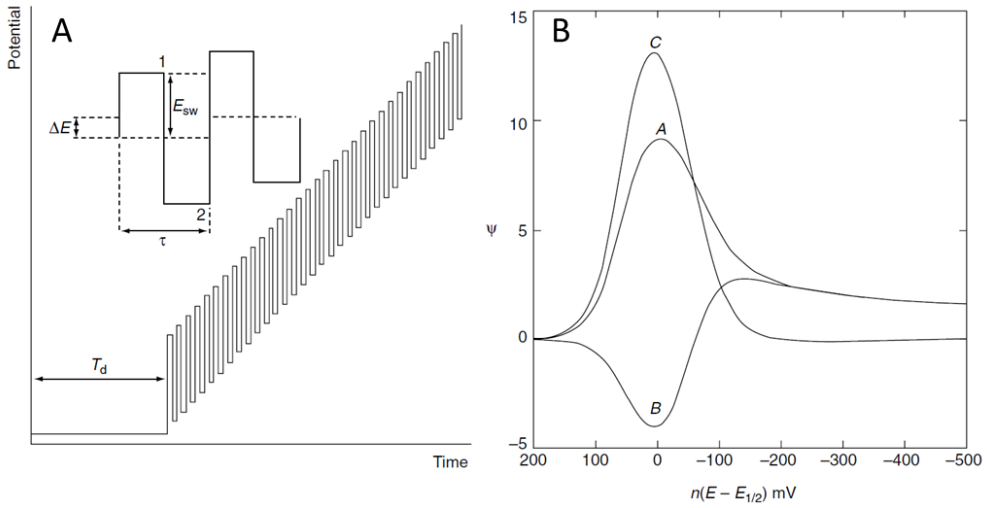

Figure 2-4: SWV of amplitude Es_w, step height ΔE, square wave period T, and delay time T_d, with the current measured at both t_1 and t_2 (A); reversible SWV in with curve A is the forward current, B is reverse current, and C is the net peak current (B).[20]

2.2 The Concept of Water Quality

It is great to see the industrial and agricultural development rise in an unprecedented level, which raise the living standards of humans. Though, as a collateral damage, the biosphere was affected first. For instance, the aquatic environment has dramatically deteriorated out of such developments. The water quality concept refers to a measurement of the extent to which water is decorous for the different living organisms uses. This concept can also be defined with regard to the existence of specific aqueous organic and inorganic nutrients in addition to certain chemical and physical properties in water.[23]

Developing countries are faced with several environmental issues, one of the most important of which is water pollution. For instance, the Egyptian Nile has been estimated to receive at least 275 million tons of industrial and organic wastes each year. Needless to say, this is a direct result of the unmonitored and unsuitable industrial and irrigation drainage systems which directly throw their waste in the Nile streams. As a result, several pollutant levels (see Figure 2-4) have raised up such as pathogens, pesticides, and heavy metal ions. For example, coke industry pumps

massive amounts of manganese waste water, while lead and zinc pollution is attributed to steel industry. It has been shown that water pollution has its direct influence on aquatic organisms, agricultural quality, and public health.[24]

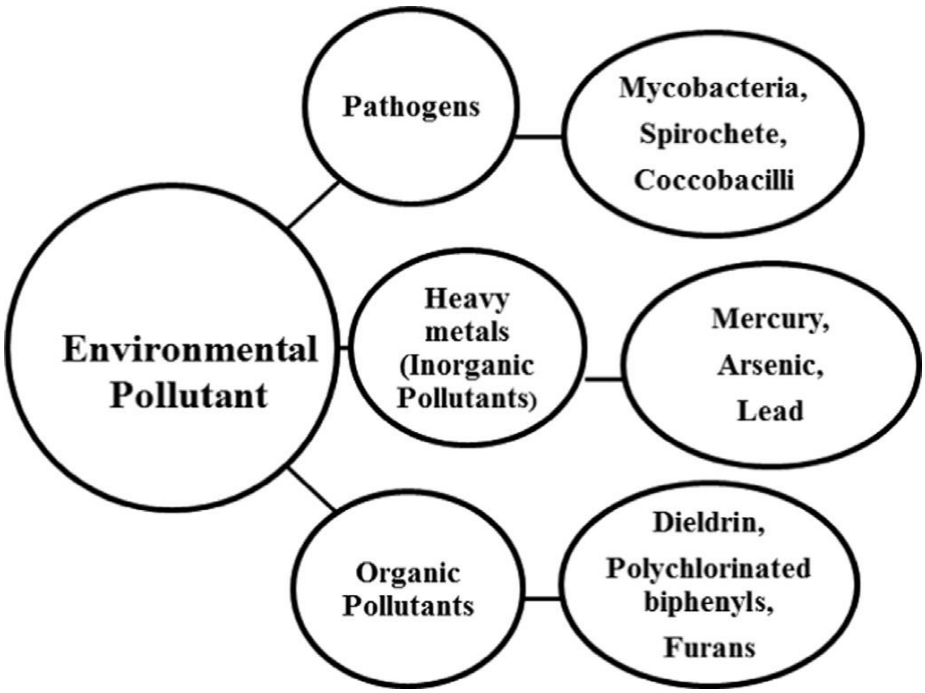

Figure 2-4: Schematic numeration of the most common water pollutants.[25]

2.2.1 Heavy Metals as Water Pollutants

Heavy metals, out of the several aquatic pollutants numerated in Figure 2-4, are of very potent effects. Numerous definitions have been proposed to describe heavy metals, such as

a. Elements whose density is greater than 5 g/cm^3.
b. Metals of atomic weight that ranges from 63.5 to 200.6 g/mol.
c. Metals that harmfully affect the biosphere and the environment.

The 'Agency for Toxic Substances and Disease Registry Priority List of Hazardous Substances' has considered heavy metals as one of the most potent

"Environmental Health Hazards". This, of course, due to the vigorous health risks and environmentally destructive effects.[17]

For many metals, it is biologically important to gain them in a nutritional trace-levels to maintain the biological systems performing efficiently such as oxygen transport and cell signaling systems. In this regard, these metals (such as Ca, Fe, and Ca) are harmful only when they exceed a certain level in the systems. Nonetheless, other metals are dangerous even at their trace levels. For example, Cd, Hg, and As have shown a powerful toxicity against living cells regardless of their concentrations. Principally, the toxicity mechanism of heavy metals depends on the destruction of the oxidative systems they cause in the living cell, which follows enzyme inhibition. This leads to extreme production of reactive oxidative species (ROS) that unswervingly changes the operation systems of DNA, proteins, and lipids. The excessive oxidation of such profound cell constituents results in cell dysfunction and then complete biological failure, as shown in Figure 2-5.[27]

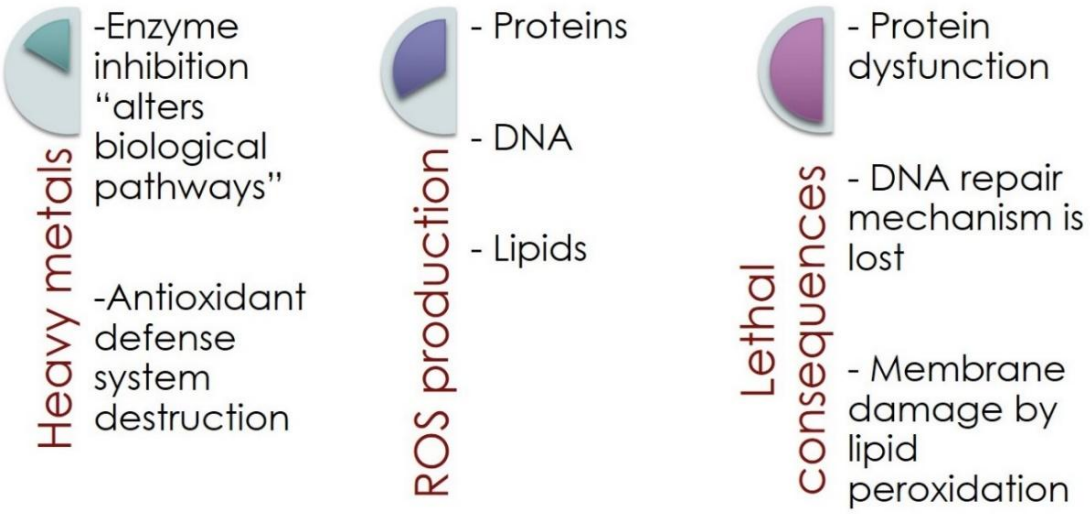

Figure 2-5: Schematic illustration of the stages of the interactive mechanism between heavy metals and the biological systems.

Mercury (Hg), in particular, is one of the ten most hazardous chemicals to the human health, according to the World's Health Organization (WHO).[28] It is an environmental pollutant heavy metal that is known for its potent toxicity towards the living organisms. As it accumulates in the food chain, Hg directly threatens the public health via damaging the kidney, liver, brain, lungs, and the cardiovascular system.[17,29] Therefore, various analytical techniques have been utilized to detect Hg^{2+} such as OES, ASF, AAS, ICP-MS, and ICP-OES.[2,30] As previously referred to, despite their sensitivity, each of these methods might have a certain drawback such as tedious sample preparation, high cost, need for well-trained personnel, time consumption, and laboratory binding.[30,31] On contrary, electrochemical techniques offer a promising alternative route that is sensitive, selective, fast, and versatile, with much less need to expensive equipment.[32] Actually, detecting Hg by the electrochemical route is recommended by the United States Environmental Protection Agency (U.S. EPA).[30] In developing countries, still, most of the daily activities primarily depend on rivers, from cleaning and drinking to waste disposal. Until a real change takes place, the concentration level of heavy metals needs to be accurately monitored around-the-clock. This will help safeguarding the vulnerable aquatic ecology from any further deterioration.

2.2.2 RGO/TNT as an Electrochemical Modifier for Hg(II) Sensing

Graphene (Gr) is a one-atom-thick single layer of carbon atoms that are sp^2-bonded and densely packed to form a lattice of a honeycomb shape.[31] In account of its excellent charge carriers' mobility,[32] high thermal and electrical conductivity,[33] very large surface area-to-volume ratio,[34] with high stiffness and strength levels,[35] Gr was utilized in various applications such as catalysis, biosensing, photo-induced energy conversion, and other electronic applications.[36,37] Using Gr in electrochemistry mostly

involve a reduction process in which its oxide form is converted into —OH, —OOH, and —COOH functional groups that enhance the absorption of analyte ions on the surface of graphene.[38,39] However, upon drying, the as-reduced sheets tend to agglomerate, or even restack into graphite, due to the van der Waal forces and π—π stacking.[40,41] Also, the strong absorption between the hydrophilic groups and analyte species can lead to low reusability of the electrode surface due to tedious desorption processes. Consequently, reduced graphene oxide (RGO) is favored in some electrochemical applications.[42]

On the other hand, owing to its nontoxicity, biocompatibility, efficient conductivity, chemical stability, eminent catalytic properties, and cost-effectiveness, titania (TiO_2) has been utilized as a superior electrode material for a variety of applications.[43–46] Among the various tailored TiO_2 nanomaterials, the one-dimensional structures have shown exceptional electrical properties, especially the nanotubular structure.[47] More specifically, well-ordered TiO_2 nanotubes (TNTs) have proven to possess an excellent charge transport and separation characteristics with a very large specific surface area and a good mechanical stability.[48] As a result, TNTs were considered as an auspicious material for a plethora of applications such as energy storage, catalytic reduction, dye-sensitized solar cells, and electrochemical sensing and biosensing.[49,50]

A number of reports have introduced Gr/TiO_2 nanocomposites for a variety of applications.[51–53] Herein, we investigated, for the first time, the applicability of RGO/TNTs nanocomposite as a chemical modifier of CPE. This mixture can offer a superior conductivity for CPE, as the agglomeration problem of graphene is minimized by the presence TiO_2, which acts as a template thanks to its nanotubular structure. This structure can also increase the charge transfer rate and the electrode

accessible surface due to its one-dimensional porous geometry.[48] Furthermore, the tedious desorption of analyte species from Gr sheets is now deviated, due to the use of RGO instead, making the platform a better reusable material.[42]

2.3 Importance of Pharmaceuticals Detection

Pharmaceuticals and personal care products (PPCP) are of the so-called "emerging contaminants". These compounds were of minimal effect in the past and only few decades ago started to emerge as potential harmful species.[54] As most of the drug dosage taken by people is disposed via urine and feces in the sewage water, these drugs find their way to plants and aquatic organisms. Absorbing them by these species may end up causing their DNA damage, fish sex exchange, and cancer, which will have its potent and direct effect towards public health.[55] In other uses, the interfering effect between drugs hinders the ability to quantify their concentration during formulation, leading to serious problems in their production lines. Also, for quality control purposes, the effective ingredients in drug formulations need to be measured in the production line. Moreover, special types of drugs, such as addictive ones, need an around-the-clock monitoring to prevent their misuse or excessive dosage. All these purposes require the presence of strict, sensitive, fast, and selective detection platforms for pharmaceuticals.[56,57]

2.3.1 Detection of Lornoxicam (LOR) in the Presence of Paracetamol (PAR)

Lornoxicam (LOR) or chlortenoxicam, chemically known as (3E)-6-chloro-3-[hydroxyl (pyridin-2-ylamino) methylene]-2-methyl-2, 3-dihydro-4H-thieno [2,3-e][1,2]thiazin-4-one 1,1-dioxide (Scheme 1), is a non-steroidal anti-inflammatory drug (NSAID).[58] It is a commonly used pain reliever for joint disorders, sciatica, and post-operative pain,[59] as it exerts its analgesic and antipyretic activities by blocking

cyclooxygenase enzyme and inhibiting the biosynthesis of prostaglandins.[60] LOR is distinguished from other oxicam derivatives by its relatively rapid onset of action, almost complete absorption from the digestive tract, and short elimination life-time (3−5 h), which make it highly tolerable.[61]

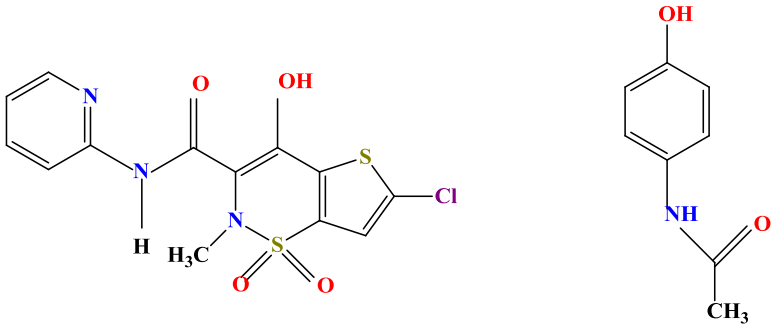

LOR **PAR**

Scheme 2.1: Chemical structures of LOR and PAR

Paracetamol (PAR), N-acetyl-p-aminophenol (Scheme 1), is also a widespread agent in pain relief medications used for headache, fever, toothache, and musculo-skeletal originated pain.[62,63] Although the general use of its normal dose is safe on public heath, long term and/or large dose therapy of PAR lead to harmful effects on vital body organs like liver, kidney and pancreas, especially when co-administered with other drugs or alcohol.[64] Therefore, the amount of PAR in pharmaceutical formulations should be strictly monitored.[64,65] Also, recent treatment trends are to utilize more than one drug in one pharmaceutical formulation, such as LOR and PAR in the same drug, making use of their synergetic effect. This makes it challenging to precisely evaluate a single component in the drug.[66] Consequently, an accurate, feasible, and fast detection of LOR, owing to its therapeutic importance, in the presence of PAR is urgently needed.

2.3.2 $BaNb_2O_6$ Nanofibers as an Electrochemical Modifier for LOR Sensing

Recently, inorganic perovskite materials have attracted the attention of the scientific community to be utilized in various catalytic and electrochemical applications, such as fuel cells, gas sensing, methane combustion, and other transduction and energy conversion applications.[67,68] This is mainly attributed to their peculiar properties, such as superconductivity, ferromagnetism, ferroelectricity, high oxygen ion mobility, charge ordering, and considerable thermopower and chemical stability.[69,70] All these characteristics reveal that perovskite structures can accommodate a variety of ions,[71] which would suggest a great potential for use as chemical modifiers for highly selective and sensitive detection of biomolecules. As new ferroelectric tungsten bronze materials, barium niobate ($BaNb_2O_6$) and its derivatives have recently attracted great interest, due to their excellent electrical conductivity, pyroelectric, and electro-optic properties.[72,73] Despite these numerous advantages, one main shortcoming of transition metal oxides is their tendency to form closely-packed aggregates on the electrode surface, which would diminish the electrochemical behavior of the sensing process.[74] Thus, electrospun perovskite nanofibers are thought to be useful, as they possess high surface area-to-volume ratio with small grain size and higher probability of charge separation, which would enhance the electrocatalytic properties of the sensor.[70] To the best of our knowledge, this is the first study on the electrochemical sensing of the mixture of LOR and PAR. To achieve this, we unprecedentedly used CPE modified with electrospun barium niobate nanofibers ($BaNb_2O_6$/CPE).

2.4 References

(1) Rodriguez, J. A.; Fernández-García, M. *Synthesis, Properties, and Applications of Oxide Nanomaterials*; John Wiley & Sons, 2007.

(2) Behbahani, M.; Esrafili, A.; Bagheri, S.; Radfar, S.; Bojdi, M. K.; Bagheri, A. Modified Nanoporous Carbon as a Novel Sorbent before Solvent-Based de-Emulsification Dispersive Liquid–liquid Microextraction for Ultra-Trace Detection of Cadmium by Flame Atomic Absorption Spectrophotometry. *Measurement* **2014**, *51*, 174–181.

(3) Sanchez-Rodas, D.; Corns, W. T.; Chen, B.; Stockwell, P. B. Atomic Fluorescence Spectrometry: A Suitable Detection Technique in Speciation Studies for Arsenic, Selenium, Antimony and Mercury. *J. Anal. At. Spectrom.* **2010**, *25* (7), 933–946.

(4) Jignesh, S.; Vineeta, K.; Abhay, S.; Vilasrao, K. Analytical Methods for Estimation of Metals. *Int.J.Res.Pharm.Chem* **2012**, *2*, 146–163.

(5) Taha, E. A.; Salama, N. N.; Fattah, L. E.-S. A. Stability-Indicating Chromatographic Methods for the Determination of Some Oxicams. *J. AOAC Int.* **2004**, *87* (2), 366–373.

(6) Jain, D. K.; Patel, P.; Chandel, H. S.; Kushwaha, A.; Jain, N. Development and Validation of Reversed Phase-High-Performance Liquid Chromatography Method for Determination of Paracetamol and Lornoxicam in Tablet Dosage Form. *Pharm. Methods* **2011**, *2* (1), 42–46.

(7) Sahoo, M.; Syal, P.; Ingale, S.; Ingale, K.; Sindhe, S.; Sali, M.; Choudhari, V. P.; Kuchekar, B. S. Development and Validation of a RP-HPLC-PDA

Method for Simultaneous Determination of Lornoxicam and Thiocolchicoside in Pharmaceutical Dosage Form and Its Application for Dissolution Study. *Int J Res Pharm Sci* **2011**, *2* (1), 1–7.

(8) Taha, E. A.; Salama, N. N.; Fattah, L. E.-S. A. Spectrofluorimetric and Spectrophotometric Stability-Indicating Methods for Determination of Some Oxicams Using 7-Chloro-4-Nitrobenz-2-Oxa-1, 3-Diazole (NBD-Cl). *Chem. Pharm. Bull.* **2006**, *54* (5), 653–658.

(9) Zhao, F.; Zhao, W. Investigation on the Micelle-Sensitized Ce (IV)-Lornoxicam-Rh B Chemiluminescence System and Its Application. *J. Fluoresc.* **2012**, *22* (1), 529–535.

(10) Akhtar, J.; Prajapati, J.; ShamimAhmad, M. M.; Elhassan, G. O. Development and Validation of Derivative Spectrophotometric Method for Simultaneous Estimation of Lornoxicam and Eperisone in Their Synthetic Mixture. *Asian J. Res. Chem.* **2015**, *8* (7), 465–471.

(11) Bozal, B.; Uslu, B. Applications of Carbon Based Electrodes for Voltammetric Determination of Lornoxicam in Pharmaceutical Dosage Form and Human Serum. *Comb. Chem. High Throughput Screen.* **2010**, *13* (7), 599–609.

(12) Bojdi, M. K.; Mashhadizadeh, M. H.; Behbahani, M.; Farahani, A.; Davarani, S. S. H.; Bagheri, A. Synthesis, Characterization and Application of Novel Lead Imprinted Polymer Nanoparticles as a High Selective Electrochemical Sensor for Ultra-Trace Determination of Lead Ions in Complex Matrixes. *Electrochim. Acta* **2014**, *136*, 59–65.

(13) Wang, J. *Analytical Electrochemistry*; John Wiley & Sons, 2006.

(14) Cui, L.; Wu, J.; Ju, H. Electrochemical Sensing of Heavy Metal Ions with Inorganic, Organic and Bio-Materials. *Biosens. Bioelectron.* **2015**, *63*, 276–286.

(15) Farghaly, O. A.; Hameed, R. S. A.; Abu-Nawwas, A.-A. H. Analytical Application Using Modern Electrochemical Techniques. *Int.J.Electrochem.Sci* **2014**, *9*, 3287–3318.

(16) Khairy, M.; Choudry, N. A.; Ouasti, M.; Kampouris, D. K.; Kadara, R. O.; Banks, C. E. Gold Nanoparticle Ensembles Allow Mechanistic Insights into Electrochemical Processes. *ChemPhysChem* **2010**, *11* (4), 875–879.

(17) Gumpu, M. B.; Sethuraman, S.; Krishnan, U. M.; Rayappan, J. B. B. A Review on Detection of Heavy Metal Ions in Water–An Electrochemical Approach. *Sensors Actuators B Chem.* **2015**, *213*, 515–533.

(18) Oyama, M. Recent Nanoarchitectures in Metal Nanoparticle-Modified Electrodes for Electroanalysis. *Anal. Sci.* **2010**, *26* (1), 1–12.

(19) Osteryoung, J. G.; Osteryoung, R. A. Square Wave Voltammetry. *Anal. Chem.* **1985**, *57* (1), 101–110.

(20) O'Dea, J. J.; Osteryoung, J.; Osteryoung, R. A. Theory of Square Wave Voltammetry for Kinetic Systems. *Anal. Chem.* **1981**, *53* (4), 695–701.

(21) Controlled-Potential Techniques. In *Analytical Electrochemistry*; John Wiley & Sons, Inc.: Hoboken, NJ, USA, 2006; pp 67–114.

(22) Zachowski, E. J.; Wojciechowski, M.; Osteryoung, J. The Analytical Application of Square-Wave Voltammetry. *Anal. Chim. Acta* **1986**, *183*, 47–57.

(23) Mapfumo, E.; Willms, W. D.; Chanasyk, D. S. Water Quality of Surface Runoff from Grazed Fescue Grassland Watersheds in Alberta. *Water Qual. Res. J. Canada* **2002**, *37* (3), 543–562.

(24) El-Sheekh, M. M. Impact of Water Quality on Ecosystems of the Nile River. **2016**.

(25) Zaib, M.; Athar, M. M.; Saeed, A.; Farooq, U. Electrochemical Determination of Inorganic Mercury and Arsenic—A Review. *Biosens. Bioelectron.* **2015**, *74*, 895–908.

(26) Valko, M.; Morris, H.; Cronin, M. T. D. Metals, Toxicity and Oxidative Stress. *Curr. Med. Chem.* **2005**, *12* (10), 1161–1208.

(27) Flora, S. J. Structural, Chemical and Biological Aspects of Antioxidants for Strategies against Metal and Metalloid Exposure. *Oxid. Med. Cell. Longev.* **2009**, *2* (4), 191–206.

(28) Edition, F. Guidelines for Drinking-Water Quality. *WHO Chron.* **2011**, *38*, 104–108.

(29) Jiang, Y.; He, T.; Chen, Y.; Ruan, Y.; Zhou, Y.; Tang, B. Z.; Qin, J.; Tang, Y. Quantitative Evaluation and in Vivo Visualization of Mercury Ion Bioaccumulation in Rotifers by Novel Aggregation-Induced Emission Fluorogen Nanoparticles. *Environ. Sci. Nano* **2017**.

(30) Martín-Yerga, D.; González-García, M. B.; Costa-García, A. Electrochemical Determination of Mercury: A Review. *Talanta* **2013**, *116*, 1091–1104.

(31) Zhang, X.; Cui, X. Graphene/Semiconductor Nanocomposites: Preparation and Application for Photocatalytic Hydrogen Evolution. *Nanocomposites-New Trends Dev. InTech, Rijeka, Croat.* **2012**, 243.

(32) Bolotin, K. I.; Sikes, K. J.; Jiang, Z.; Klima, M.; Fudenberg, G.; Hone, J.; Kim, P.; Stormer, H. L. Ultrahigh Electron Mobility in Suspended Graphene. *Solid State Commun.* **2008**, *146* (9), 351–355.

(33) Balandin, A. A.; Ghosh, S.; Bao, W.; Calizo, I.; Teweldebrhan, D.; Miao, F.; Lau, C. N. Superior Thermal Conductivity of Single-Layer Graphene. *Nano Lett.* **2008**, *8* (3), 902–907.

(34) Mohamed, M. A.; Atty, S. A.; Salama, N. N.; Banks, C. E. Highly Selective Sensing Platform Utilizing Graphene Oxide and Multiwalled Carbon Nanotubes for the Sensitive Determination of Tramadol in the Presence of Co- Formulated Drugs. *Electroanalysis* **2017**, *29* (4), 1038–1048.

(35) Lee, J.-U.; Yoon, D.; Cheong, H. Estimation of Young's Modulus of Graphene by Raman Spectroscopy. *Nano Lett.* **2012**, *12* (9), 4444–4448.

(36) Avouris, P. Graphene: Electronic and Photonic Properties and Devices. *Nano Lett.* **2010**, *10* (11), 4285–4294.

(37) Mohamed, M. A.; Yehia, A. M.; Banks, C. E.; Allam, N. K. Novel MWCNTs/Graphene Oxide/Pyrogallol Composite with Enhanced Sensitivity for Biosensing Applications. *Biosens. Bioelectron.* **2017**, *89*, 1034–1041.

(38) Du, D.; Liu, J.; Zhang, X.; Cui, X.; Lin, Y. One-Step Electrochemical Deposition of a Graphene-ZrO_2 Nanocomposite: Preparation, Characterization and

Application for Detection of Organophosphorus Agents. *J. Mater. Chem.* **2011**, *21* (22), 8032–8037.

(39) Klunk, W. E.; Koeppe, R. A.; Price, J. C.; Benzinger, T. L.; Devous MD, S.; Jagust, W. J.; Johnson, K. A.; Mathis, C. A.; Minhas, D.; Pontecorvo, M. J.; et al. The Centiloid Project: Standardizing Quantitative Amyloid Plaque Estimation by PET. *Alzheimers. Dement.* **2015**, *11* (1), 1–4.

(40) Liu, J.; Fu, S.; Yuan, B.; Li, Y.; Deng, Z. Toward a Universal "Adhesive Nanosheet" for the Assembly of Multiple Nanoparticles Based on a Protein-Induced Reduction/Decoration of Graphene Oxide. *J. Am. Chem. Soc.* **2010**, *132* (21), 7279–7281.

(41) Sun, Y.; Yan, K.; Wang, G.; Guo, W.; Ma, T. Effect of Annealing Temperature on the Hydrogen Production of TiO_2 Nanotube Arrays in a Two-Compartment Photoelectrochemical Cell. *J. Phys. Chem. C* **2011**, *115* (26), 12844–12849.

(42) Wei, Y.; Gao, C.; Meng, F.-L.; Li, H.-H.; Wang, L.; Liu, J.-H.; Huang, X.-J. SnO2/Reduced Graphene Oxide Nanocomposite for the Simultaneous Electrochemical Detection of Cadmium (II), Lead (II), Copper (II), and Mercury (II): An Interesting Favorable Mutual Interference. *J. Phys. Chem. C* **2011**, *116* (1), 1034–1041.

(43) Zhu, Y.; Cao, H.; Tang, L.; Yang, X.; Li, C. Immobilization of Horseradish Peroxidase in Three-Dimensional Macroporous TiO_2 Matrices for Biosensor Applications. *Electrochim. Acta* **2009**, *54* (10), 2823–2827.

(44) Singh, P.; Kumar, A.; Kaur, D. Substrate Effect on Texture Properties of Nanocrystalline TiO_2 Thin Films. *Phys. B Condens. Matter* **2008**, *403* (19), 3769–3773.

(45) Hegazy, A.; Kinadjian, N.; Sadeghimakki, B.; Sivoththaman, S.; Allam, N. K.; Prouzet, E. TiO_2 Nanoparticles Optimized for Photoanodes Tested in Large Area Dye-Sensitized Solar Cells (DSSC). *Sol. Energy Mater. Sol. Cells* **2016**, *153*, 108–116.

(46) Ahmed, N.; Farghali, A. A.; El Rouby, W. M. A.; Allam, N. K. Enhanced Photoelectrochemical Water Splitting Characteristics of TiO_2 Hollow Porous Spheres by Embedding Graphene as an Electron Transfer Channel. *Int. J. Hydrogen Energy* **2017**, *42* (49), 29131–29139.

(47) Perillo, P. M.; Rodriguez, D. F. The Gas Sensing Properties at Room Temperature of TiO_2 Nanotubes by Anodization. *Sensors Actuators B Chem.* **2012**, *171*, 639–643.

(48) Ameen, S.; Akhtar, M. S.; Seo, H.-K.; Shin, H.-S. TiO_2 Nanotube Arrays via Electrochemical Anodic Oxidation: Prospective Electrode for Sensing Phenyl Hydrazine. *Appl. Phys. Lett.* **2013**, *103* (6), 61602.

(49) Mohamed, A. M.; Aljaber, A. S.; AlQaradawi, S. Y.; Allam, N. K. TiO_2 Nanotubes with Ultrathin Walls for Enhanced Water Splitting. *Chem. Commun.* **2015**, *51* (63), 12617–12620.

(50) Liu, N.; Chen, X.; Zhang, J.; Schwank, J. W. A Review on TiO_2-Based Nanotubes Synthesized via Hydrothermal Method: Formation Mechanism, Structure Modification, and Photocatalytic Applications. *Catal. Today* **2014**, *225*, 34–51.

(51) Fan, Y.; Lu, H.-T.; Liu, J.-H.; Yang, C.-P.; Jing, Q.-S.; Zhang, Y.-X.; Yang, X.-K.; Huang, K.-J. Hydrothermal Preparation and Electrochemical Sensing Properties of TiO_2–graphene Nanocomposite. *Colloids Surfaces B Biointerfaces* **2011**, *83* (1), 78–82.

(52) Wang, X.; Li, G.; Liu, L.; Cheng, Y.; Zheng, W.; Wu, S.; Wu, F.; Sun, W. Application of Titanium Dioxide Nanowires and Electroreduced Graphene Oxide Modified Electrodes for the Electrochemical Detection of Specific Tlh Gene Sequence from Vibrio Parahaemolyticus. *Anal. Methods* **2015**, *7* (6), 2623–2629.

(53) Li, X.; Zhao, Y.; Wang, X.; Wang, J.; Gaskov, A. M.; Akbar, S. A. Reduced Graphene Oxide (RGO) Decorated TiO_2 Microspheres for Selective Room-Temperature Gas Sensors. *Sensors Actuators B Chem.* **2016**, *230*, 330–336.

(54) Jurado, A.; Vàzquez-Suñé, E.; Carrera, J.; López de Alda, M.; Pujades, E.; Barceló, D. Emerging Organic Contaminants in Groundwater in Spain: A Review of Sources, Recent Occurrence and Fate in a European Context. *Sci. Total Environ.* **2012**, *440*, 82–94.

(55) Angnes, L. Pharmaceuticals and Personal Care Products; 2015; pp 881–903.

(56) Moretto, L. Environmental Analysis by Electrochemical Sensors and Biosensors.; Springer-Verlag New York, 2016.

(57) Chitravathi, S.; Munichandraiah, N. Voltammetric Determination of Paracetamol, Tramadol and Caffeine Using Poly (Nile Blue) Modified Glassy Carbon Electrode. *J. Electroanal. Chem.* **2016**, *764*, 93–103.

(58) Balfour, J. A.; Fitton, A.; Barradell, L. B. Lornoxicam. *Drugs* **1996**, *51* (4), 639–657.

(59) Das, S. K.; Banerjee, M.; Mondal, S.; Ghosh, B.; Ghosh, B.; Sen, S. A Comparative Study of Efficacy and Safety of Lornoxicam versus Tramadol as Analgesics after Surgery on Head and Neck. *Indian J. Otolaryngol. Head Neck Surg.* **2013**, *65* (1), 126–130.

(60) Bianchi, M.; Panerai, A. E. Effects of Lornoxicam, Piroxicam, and Meloxicam in a Model of Thermal Hindpaw Hyperalgesia Induced by Formalin Injection in Rat Tail. *Pharmacol. Res.* **2002**, *45* (2), 101–105.

(61) Xiao, B.; Zhao, F.; Gao, Y. Characterization and Application of Lornoxicam, Europium (III), and Lysozyme Fluorescence. *Instrum. Sci. Technol.* **2016**, *44* (3), 282–293.

(62) Attimarad, M. Simultaneous Determination of Paracetamol and Lornoxicam by RP-HPLC in Bulk and Tablet Formulation. *Pharm. Methods* **2011**, *2* (1), 61–66.

(63) Mohamed, M. A.; El-Gendy, D. M.; Ahmed, N.; Banks, C. E.; Allam, N. K. 3D Spongy Graphene-Modified Screen-Printed Sensors for the Voltammetric Determination of the Narcotic Drug Codeine. *Biosens. Bioelectron.* **2018**, *101*, 90–95.

(64) Martin, F. L.; McLean, A. E. M. Comparison of Paracetamol-Induced Hepatotoxicity in the Rat in Vivo with Progression of Cell Injury in Vitro in Rat Liver Slices. *Drug Chem. Toxicol.* **1998**, *21* (4), 477–494.

(65) Lourencao, B. C.; Medeiros, R. A.; Rocha-Filho, R. C.; Mazo, L. H.; Fatibello-Filho, O. Simultaneous Voltammetric Determination of Paracetamol and

Caffeine in Pharmaceutical Formulations Using a Boron-Doped Diamond Electrode. *Talanta* **2009**, *78* (3), 748–752.

(66) Kumar Talluri, M. V. N.; Bairwa, M. K.; Theja Dugga, H. H.; Srinivas, R. Development and Validation of RP-HPLC and Ultraviolet Spectrophotometric Methods of Analysis for Simultaneous Determination of Paracetamol and Lornoxicam in Pharmaceutical Dosage Forms. *J. Liq. Chromatogr. Relat. Technol.* **2012**, *35* (1), 129–140.

(67) Zhu, H.; Zhang, P.; Dai, S. Recent Advances of Lanthanum-Based Perovskite Oxides for Catalysis. *ACS Catal.* **2015**, *5* (11), 6370–6385.

(68) Abdellah, A. M.; Hafez, A.; Panikkanvalappil, S. R.; El-Sayed, M. A.; Allam, N. K. Single-Crystal Electrospun Plasmonic Perovskite Nanofibers. *J. Phys. Chem. C* **2018**, *122*, 27.

(69) Kießling, D.; Schneider, R.; Kraak, P.; Haftendorn, M.; Wendt, G. Perovskite-Type Oxides–catalysts for the Total Oxidation of Chlorinated Hydrocarbons. *Appl. Catal. B Environ.* **1998**, *19* (2), 143–151.

(70) Wang, B.; Gu, S.; Ding, Y.; Chu, Y.; Zhang, Z.; Ba, X.; Zhang, Q.; Li, X. A Novel Route to Prepare $LaNiO_3$ Perovskite-Type Oxide Nanofibers by Electrospinning for Glucose and Hydrogen Peroxide Sensing. *Analyst* **2013**, *138* (1), 362–367.

(671) Jia, F.-F.; Zhong, H.; Zhang, W.-G.; Li, X.-R.; Wang, G.-Y.; Song, J.; Cheng, Z.-P.; Yin, J.-Z.; Guo, L.-P. A Novel Nonenzymatic ECL Glucose Sensor Based on Perovskite $LaTiO_3$-Ag0.1 Nanomaterials. *Sensors Actuators B Chem.* **2015**, *212*, 174–182.

(72) Gao, P.; Pu, Y.; Li, P.; Wu, T. Effects of $BaNb_2O_6$ Addition on Microstructure and Dielectric Properties of $BaTiO_3$ Ceramics. *J. Mater. Sci. Mater. Electron.* **2013**, *24* (10), 3958–3962.

(73) Chan, J. H.; Bock, J. A.; Guo, H.; Trolier- McKinstry, S.; Randall, C. A. Filled Oxygen- deficient Strontium Barium Niobates. *J. Am. Ceram. Soc.* **2017**, *100* (2), 774–782.

(74) Liu, G.; Zhong, H.; Li, X.; Yang, K.; Jia, F.; Cheng, Z.; Zhang, L.; Yin, J.; Guo, L.; Qian, H. Research on Nonenzymatic Electrochemical Sensor Using HO-$BiONO_3$ Nanocomposites for Glucose Detection. *Sensors Actuators B Chem.* **2017**, *242*, 484–491.

Chapter 3

Literature Survey

Decades ago, research has started to develop sensors to monitor the vital parameters that need around-the-clock detection in order to interfere at the right time and prevent possible deterioration. This has been applied on environmental, pharmaceutical, medical, electronic, and food goods levels, along with many others. The aim was always to control their quality and ensure that undesirable species are always within the permissible limits. As we are interested in heavy metal and pharmaceutical sensing, the following is a literature review of some recent studies in these fields.

3.1 Heavy Metals Detection

As previously mentioned, for electrochemical sensors to operate as selectively and sensitively as possible, trends have been toward modifying the surface. Nanostructures can significantly change the materials behavior as it is governed by quantum chemistry and have high surface area to volume ratio (SA/V). For this, many of the recent effective modifications involve such structures to improve their sensitivity. The following are some of these studies.

3.1.1 Metallic Nanostructured Materials

Metallic nanostructures have been thoroughly studied for electrochemical modification purposes showing a promising performance. This is mainly owing to their superior electrical conductivity and the ability to bind to the targeted ions. Therefore, nanostructured metals possess an extraordinary tendency to attract the targeted ions during preconcentration step onto their surfaces. Statistically speaking,

mercury is one of the most common metallic modifiers used for detection purposes. Later on, it will be shown how mercury is also used for pharmaceuticals detection. Nonetheless, as mercury itself is toxic, it is better to be changed with harmless alternatives. Examples for candidates are silver, gold, antimony, and bismuth.[1]

In particular, Au nanostructures are of the most extensively studied modifiers for a sensitive electrochemical process. That is attributed to their large surface area and high catalytic activity, electrical conductivity, and ease of deposition. Recent studies used deposited Au nanoparticles on electrodes of quartz crystal microbalance (QCM) for selective detection of Hg in which LOD was 22 $\mu g/m^3$.[2] Au-NPs have been deposition for detection of other metals such as Pb(II), Cu(II), Fe(III), and Cd(II) ions.[3,4] In some cases, the limit of detection (LOD) was as low as 100 fM.[5] Despite of this very low detection limit, the use of Au as a modifier is still restricted by its high cost.

In the same manner, morphologically self-ordered Bi nanostructures were proved to possess a great sensitivity to heavy metal ions. Several structures have been utilized to modify carbon electrodes for detection of metal ions such as Cd(II) and Pb(II).[6,7] These structures exhibited a huge surface free energy along with their large surface-area-to-volume ratio. Such characteristics were why Bi-modified working electrode demonstrate a distinguishing adsorbability towards its targeted ions achieving an LOD of 12 nM. Bi-modified electrodes can also instantaneously sensitively detect Hg^{2+}, Cu^{2+}, and Cd^{2+} ions, but not to a competitive enough LOD. However, some important experimental parameters in the detection process still need to be scrutinized such as selectivity and reproducibilty.[8] BiNPs have been also studied for electrodeposition on carbon electrodes to detect heavy metal ions using square

wave anodic stripping voltammetry (SWASV) technique. The detection limits were in the range of 10^{-7} g/L.[9]

More chances to enhance the accuracy of the electrochemical sensing process can be offered by using of bimetallic nanomaterials. That is mainly attributed to the fact that bimetallics try to gather the merits of both metals involved and recuperate the shortcomings of each one by its counterpart.[10,11] For instance, Au-Pt nanoparticles have been utilized for such an application, which lead to a sensitivity of 0.008 ppb against Hg^{2+}. In addition to its sensitivity, the proposed bimetallic sensing platform modifier exhibited low interference chances in solutions containing Cu^{2+}, Mn^{2+}, Zn^{2+}, Cr^{3+}, and Co^{2+} ions.[8,12]

3.1.2 Carbon-based Nanostructured Materials

A superior electrochemical performance has been exhibited by carbonic materials to act in both adsorption and transduction. As a result, carbonic structures such as graphene (Gr), reduced graphene oxide (RGO), and carbon nanotubes (CNTs) have been extensively during the past few decades.[2] Largely, CPE is a unique carbonic heterogeneous electrode in which graphite powder is mixed with a water-immiscible non-conductive binder, such as paraffin oil.[13] The easy functionalization of CPEs helped involving them in many studies to enhance the electrocatalytic activity for various purposes, by improving the charge transfer kinetics.[14] Furthermore, the chemical functionalization of CPEs has displayed electrochemical results of low noise, easy surface renewability, broad range of potential window, and low cost.[15] Therefore, chemically-functionalized CPEs with materials such as zeolites, nanostructured metallics, and biomolecules attracted the interest of the scientific community to be used for diverse electroanalytical studies.[16]

Many materials have been utilized to functionalize CPEs, one of which is carbonic materials, such as CNTs. They, CNTs, are commonly used for such an application due to their improved electrocatalytic properties and immense surface-area-to-volume ratio. Furthermore, to functionalize CNTs would enhance their sensitivity towards heavy metal ions and decrease the process time.[2] For instance, a facile preparation of 3D Graphene and MWCNTs as a glassy carbon electrode (GCE) modifier has resulted in superior Cd(II) and Pb(II) detection.[17] CNT threads and amino-functionalized carbon NPs have been also utilized for detection of several heavy metal ions such as Zn(II), Pb(II), Cu(II), and Hg(II) using ASV. The modified electrodes have resulted in superior sensitivity and selectivity.[18,19] Correspondingly, Afkhami et al[20] modified CPE performance against heavy metal ions using of Schiff base-functionalized MWCNTs. Schiff base holds the ability to form metal ion complexes, which facilitated the combination of these ions with CNTs, resulting in a high electrochemical output signal. Accordingly, the detection limit of Hg(II) was 0.9 nM and that of Pb(II) was 0.6 nM with low interference chances. Better-suited geometries to enhance the CNTs' detection performance were also studied. In one interesting study, Guo et al. fabricated vastly aligned CNT towers as an electrochemical electrode modifier to detect low concentrations of Cd^{2+}, Pb^{2+}, Cu^{2+}, and Zn^{2+}. Each CNT tower contained almost 25 million organized long CNT which produced a more efficient electroconductivity. The modification helped to achieve individual LODs of 12, 25, 44 and 67 nM for Pb^{2+}, Cd^{2+}, Cu^{2+}, and Zn^{2+} respectively.[21]

3.2 Pharmaceuticals Detection

3.2.1 Conventional Analyses

The need for detection of pharmaceuticals has relatively recently emerged, almost started in 1990s. This was not the sensing trend before as most of sensors were directed towards monitoring other organic and inorganic pollutants such as heavy metals and pesticides owing to the industrial revolution.[22] However, the exponential mechanized food production and the development of drug industry have caused drug detection to be an emerging need. In addition, drug interreference in the biological system and the wrong use of drugs for addiction purposes necessitates the need to develop effective and rapid methods of drug detection. Pharmaceuticals are rapidly increasing in numbers in which they now are exceeding 3,000 active compounds, which makes the detection process more challenging.

Plethora of studies and reviews have been published to introduce and develop solutions for pharmaceutical determination using different techniques.[23,24] As previously mentioned, this includes HPLC, ultraperformance liquid chromatography-mass spectrometry (UPLC-MS/MS), solid phase extraction-liquid chromatography–electrospray-tandem mass spectrometry (SPE-LC-ESI-MS/MS), and many other approaches.[25]

3.2.2 Electrochemical Analysis

Electrochemical analyses, especially the voltammetric ones, are well-established in the field of molecular monitoring. Many of these studies were directed towards detection of pharmaceuticals, especially in their unprocessed or commercial form.[26] A series of manuscripts have reviewed and studied the electroanalysis of pharmaceuticals via chemical modification of electrodes, which showed a great

potential to reach an acceptable sensitivity and LOD values. The following sections displays several electrode types and their use in such a purpose.[27,28]

3.2.2.1 Metallic Electrodes

Mercury electrodes, as the most used metallic electrodes in the literature, were of the first tools to use in the electroanalyses, starting by 1922. Advantages as its excellent surface renewability, hydrogen reduction overpotential, and smooth surface made hanging mercury drop electrode (HMDE) a good candidate for use as a sensor for pharmaceuticals concentration.[29] Using square wave voltammetry (SWV), HMDE was used for detection of several drugs such as triamcinolone acetonide (TAA), haloperidol, ethinylestradiol, griseofulvin, and cefoperazone. The limit of quantitation (LOQ) in each study was down to few hundred picomolar. Some of these studies required a preconcentration step (in a range of tens of seconds), and they were tried in both spiked aqueous and serum solutions.[30–32] In spite of these tremendous results, mercury electrodes still have the disadvantage of being toxic so, in case of their leakage, the results cannot be fully trusted, and the sample is not safe. This would hinder their practical use for *in-situ* applications.

One major disadvantage of using any of these solid electrodes rather than mercury is their challenging renewable surface and low chances of reproducibility. Other metallic electrodes used for pharmaceuticals detection includes gold, bismuth, copper, and palladium.[33,34] Gold electrodes, for instance, can easily be self-assembled on electrode surfaces to reach LOQ down to nanomolar level.[35] Also, bismuth film electrodes have been developed as an alternative for mercury electrodes for in situ detection of compounds such as vitamin B-12 and sildenafil citrate. The level of sensitivity was in the tens of nanomolar order.[36,37]

3.2.2.2 Carbon Electrodes

Owing to their easy handling, broad potential windows, and good conductivity, and high signal-to-noise ratio, carbon electrodes are generally good candidates for electrochemical detection. Using different electrochemical techniques such as SWV and differential pulse voltammetry (DVP), electrodes such as GCEs were used for detection of drugs such as levofloxacin, trimetazidine, and amlodipine besylate. The LODs were in the order of 10^{-10} and the linear ranged was between the milli and nano levels.[38–40] Screen printed electrodes (SPE) were recently used for medical detection purposes to introduce a new concept to analysis, Lab-On-a-Chip. Without noticeable interference, studies have employed SPEs for quantification of pharmaceuticals such as sildenafil and methionine in multispiked urine samples, in which LOQ attained 10^{-8} and 10^{-6-} M, respectively.[41,42] Other studies have reported modifications like using of 3D-spongy graphene and Cs-Au nanoparticles as modifier for detection of Codeine and Dapoxetine, respectively.[43,44]

After Adams introduced them in 1958, CPEs have been widely used for electroanalytical objectives. This is due to their versatility, easy surface renewability, feasible modification, and cost effectiveness. For drug quantification, researchers have modified CPE surface by several organic and inorganic compounds, especially the nanostructured ones. Examples are using of Graphene Oxide Nanosheets (GO), Nanocrystalline Zeolite, and Nickel Nanoparticles for determination of Ezogabine, Ledipasvir, and Escitalopram Oxalate, respectively. LOD of each of these studies was always lower than an order of 10^{-7}, especially in cospiked formulation.[45–47] Other electrodes such as silver amalgam and molecular imprinting polymers were also used for the same aim of pharmaceutical sensing, achieving a detection limit in the range of 10^{-10} M.[48]

3.3 References

(1) Svobodova-Tesarova, E.; Baldrianova, L.; Stoces, M.; Svancara, I.; Vytras, K.; Hocevar, S. B.; Ogorevc, B. Antimony Powder-Modified Carbon Paste Electrodes for Electrochemical Stripping Determination of Trace Heavy Metals. *Electrochim. Acta* **2011**, *56* (19), 6673–6677.

(2) Waheed, A.; Mansha, M.; Ullah, N. Nanomaterials-Based Electrochemical Detection of Heavy Metals in Water: Current Status, Challenges and Future Direction. *TrAC Trends Anal. Chem.* **2018**, *105*, 37–51.

(3) Zhang, B.; Chen, J.; Zhu, H.; Yang, T.; Zou, M.; Zhang, M.; Du, M. Facile and Green Fabrication of Size-Controlled AuNPs/CNFs Hybrids for the Highly Sensitive Simultaneous Detection of Heavy Metal Ions. *Electrochim. Acta* **2016**, *196*, 422–430.

(4) Zhu, Y.; Pan, D.; Hu, X.; Han, H.; Lin, M.; Wang, C. An Electrochemical Sensor Based on Reduced Graphene Oxide/Gold Nanoparticles Modified Electrode for Determination of Iron in Coastal Waters. *Sensors Actuators B Chem.* **2017**, *243*, 1–7.

(5) Suherman, A. L.; Kuss, S.; Tanner, E. E. L.; Young, N. P.; Compton, R. G. Electrochemical Hg^{2+} Detection at Tannic Acid-Gold Nanoparticle Modified Electrodes by Square Wave Voltammetry. *Analyst* **2018**, *143* (9), 2035–2041.

(6) Shi, L.; Li, Y.; Rong, X.; Wang, Y.; Ding, S. Facile Fabrication of a Novel 3D Graphene Framework/Bi Nanoparticle Film for Ultrasensitive Electrochemical Assays of Heavy Metal Ions. *Anal. Chim. Acta* **2017**, *968*, 21–29.

(7) Cui, L.; Wu, J.; Ju, H. Synthesis of Bismuth-Nanoparticle-Enriched Nanoporous Carbon on Graphene for Efficient Electrochemical Analysis of Heavy-Metal Ions. *Chem. - A Eur. J.* **2015**, *21* (32), 11525–11530.

(8) Gong, J.; Zhou, T.; Song, D.; Zhang, L.; Hu, X. Stripping Voltammetric Detection of Mercury (II) Based on a Bimetallic Au−Pt Inorganic−Organic Hybrid Nanocomposite Modified Glassy Carbon Electrode. *Anal. Chem.* **2009**, *82* (2), 567–573.

(9) Yang, D.; Wang, L.; Chen, Z.; Megharaj, M.; Naidu, R. Voltammetric Determination of Lead (II) and Cadmium (II) Using a Bismuth Film Electrode Modified with Mesoporous Silica Nanoparticles. *Electrochim. Acta* **2014**, *132*, 223–229.

(10) Kempahanumakkagari, S.; Deep, A.; Kim, K.-H.; Kumar Kailasa, S.; Yoon, H.-O. Nanomaterial-Based Electrochemical Sensors for Arsenic - A Review. *Biosens. Bioelectron.* **2017**, *95*, 106–116.

(11) Barton, J.; García, M. B. G.; Santos, D. H.; Fanjul-Bolado, P.; Ribotti, A.; McCaul, M.; Diamond, D.; Magni, P. Screen-Printed Electrodes for Environmental Monitoring of Heavy Metal Ions: A Review. *Microchim. Acta* **2016**, *183* (2), 503–517.

(12) Cui, L.; Wu, J.; Ju, H. Electrochemical Sensing of Heavy Metal Ions with Inorganic, Organic and Bio-Materials. *Biosens. Bioelectron.* **2015**, *63*, 276–286.

(13) Nossol, E.; Zarbin, A. J. G. Carbon Paste Electrodes Made from Novel Carbonaceous Materials: Preparation and Electrochemical Characterization. *Electrochim. Acta* **2008**, *54* (2), 582–589.

(14) Amiri, M.; Salehniya, H.; Habibi-Yangjeh, A. Graphitic Carbon Nitride/Chitosan Composite for Adsorption and Electrochemical Determination of Mercury in Real Samples. *Ind. Eng. Chem. Res.* **2016**, *55* (29), 8114–8122.

(15) Amiri, M.; Rezapour, F.; Bezaatpour, A. Hydrophilic Carbon Nanoparticulates at the Surface of Carbon Paste Electrode Improve Determination of Paracetamol, Phenylephrine and Dextromethorphan. *J. Electroanal. Chem.* **2014**, *735*, 10–18.

(16) Amiri, M.; Sohrabnezhad, S.; Rahimi, A. Nickel (II) Incorporated AlPO-5 Modified Carbon Paste Electrode for Determination of Thioridazine in Human Serum. *Mater. Sci. Eng. C* **2014**, *37*, 342–347.

(17) Huang, H.; Chen, T.; Liu, X.; Ma, H. Ultrasensitive and Simultaneous Detection of Heavy Metal Ions Based on Three-Dimensional Graphene-Carbon Nanotubes Hybrid Electrode Materials. *Anal. Chim. Acta* **2014**, *852*, 45–54.

(18) Zhao, D.; Guo, X.; Wang, T.; Alvarez, N.; Shanov, V. N.; Heineman, W. R. Simultaneous Detection of Heavy Metals by Anodic Stripping Voltammetry Using Carbon Nanotube Thread. *Electroanalysis* **2014**, *26* (3), 488–496.

(19) Sun, Y.-F.; Zhao, L.-J.; Jiang, T.-J.; Li, S.-S.; Yang, M.; Huang, X.-J. Sensitive and Selective Electrochemical Detection of Heavy Metal Ions Using Amino-Functionalized Carbon Microspheres. *J. Electroanal. Chem.* **2016**, *760*, 143–150.

(20) Afkhami, A.; Bagheri, H.; Khoshsafar, H.; Saber-Tehrani, M.; Tabatabaee, M.; Shirzadmehr, A. Simultaneous Trace-Levels Determination of Hg (II) and Pb (II) Ions in Various Samples Using a Modified Carbon Paste Electrode

Based on Multi-Walled Carbon Nanotubes and a New Synthesized Schiff Base. *Anal. Chim. Acta* **2012**, *746*, 98–106.

(21) Gutierrez, F. A.; Gonzalez-Dominguez, J. M.; Ansón-Casaos, A.; Hernández-Ferrer, J.; Rubianes, M. D.; Martínez, M. T.; Rivas, G. Single-Walled Carbon Nanotubes Covalently Functionalized with Cysteine: A New Alternative for the Highly Sensitive and Selective Cd(II) Quantification. *Sensors Actuators B Chem.* **2017**, *249*, 506–514.

(22) Petrovic, M.; Radjenovic, J.; Postigo, C.; Kuster, M.; Farre, M.; Alda, M. L.; Barceló, D. Emerging Contaminants in Waste Waters: Sources and Occurrence. In *Emerging Contaminants from Industrial and Municipal Waste*; Springer Berlin Heidelberg: Berlin, Heidelberg; pp 1–35.

(23) Forraz, N.; Wright, K. E.; Jurga, M.; Mcguckin, C. P. Experimental Therapies for Repair of the Central Nervous System : Stem Cells and Tissue Engineering. No. March 2012, 523–536.

(24) Universidad de Antioquia. Facultad de Química Farmacéutica., J. F.; JIMENEZ C., C. *Vitae.*; Facultad De Química Farmacéutica, Universidad de Antioquia, 2012; Vol. 19.

(25) Angnes, L. Pharmaceuticals and Personal Care Products; 2015; pp 881–903.

(26) Moretto, L. Environmental Analysis by Electrochemical Sensors and Biosensors.; Springer-Verlag New York, 2016.

(27) Uslu, B.; Ozkan, S. A. Electroanalytical Methods for the Determination of Pharmaceuticals: A Review of Recent Trends and Developments. *Anal. Lett.* **2011**, *44* (16), 2644–2702.

(28) Radi, A.-E. Recent Updates of Chemically Modified Electrodes in Pharmaceutical Analysis. *Comb. Chem. High Throughput Screen.* **2010**, *13* (8), 728–752.

(29) Duncan, J. B.; Christian, J. E. Polarographic Determination of Folic Acid and Zinc Salts in Pharmaceuticals. *J. Am. Pharm. Assoc. (Scientific ed.)* **1948**, *37* (12), 507–509.

(30) El-Desoky, H. S.; Ghoneim, M. M. Assay of the Anti-Psychotic Drug Haloperidol in Bulk Form, Pharmaceutical Formulation and Biological Fluids Using Square-Wave Adsorptive Stripping Voltammetry at a Mercury Electrode. *J. Pharm. Biomed. Anal.* **2005**, *38* (3), 543–550.

(31) Ghoneim, E. M.; El-Desoky, H. S.; Ghoneim, M. M. Adsorptive Cathodic Stripping Voltammetric Assay of the Estrogen Drug Ethinylestradiol in Pharmaceutical Formulation and Human Plasma at a Mercury Electrode. *J. Pharm. Biomed. Anal.* **2006**, *40* (2), 255–261.

(32) Hammam, E.; El-Attar, M. A.; Beltagi, A. M. Voltammetric Studies on the Antibiotic Drug Cefoperazone: Quantification and Pharmacokinetic Studies. *J. Pharm. Biomed. Anal.* **2006**, *42* (4), 523–527.

(33) Muñoz, R. A. A.; Matos, R. C.; Angnes, L. Amperometric Determination of Dipyrone in Pharmaceutical Formulations with a Flow Cell Containing Gold Electrodes from Recordable Compact Discs. *J. Pharm. Sci.* **2001**, *90* (12), 1972–1977.

(34) Peverly, A. A.; Peters, D. G. Electrochemical Determination of Trihalomethanes in Water by Means of Stripping Analysis. *Anal. Chem.* **2012**, *84* (14), 6110–6115.

(35) Masawat, P.; Slater, J. M. The Determination of Tetracycline Residues in Food Using a Disposable Screen-Printed Gold Electrode (SPGE). *Sensors Actuators B Chem.* **2007**, *124* (1), 127–132.

(36) Kreft, G. L.; de Braga, O. C.; Spinelli, A. Analytical Electrochemistry of Vitamin B12 on a Bismuth-Film Electrode Surface. *Electrochim. Acta* **2012**, *83*, 125–132.

(37) Sopha, H.; Hocevar, S. B.; Pihlar, B.; Ogorevc, B. *Electrochimica Acta.*; Elsevier Ltd, 2012; Vol. 60.

(38) Radi, A.; El-Sherif, Z. Determination of Levofloxacin in Human Urine by Adsorptive Square-Wave Anodic Stripping Voltammetry on a Glassy Carbon Electrode. *Talanta* **2002**, *58* (2), 319–324.

(39) Ghoneim, M. .; Khashaba, P. .; Beltagi, A. . Determination of Trimetazidine HCl by Adsorptive Stripping Square-Wave Voltammetry at a Glassy Carbon Electrode. *J. Pharm. Biomed. Anal.* **2002**, *27* (1–2), 235–241.

(40) Gazy, A. A. K. Determination of Amlodipine Besylate by Adsorptive Square-Wave Anodic Stripping Voltammetry on Glassy Carbon Electrode in Tablets and Biological Fluids. *Talanta* **2004**, *62* (3), 575–582.

(41) Org, W. E.; Farghali, R. A.; Ahmed, R. A. ELECTROCHEMICAL SCIENCE A Novel Electrochemical Sensor for Determination of Sildenafil Citrate

(Viagra) in Pure Form and in Biological and Pharmaceutical Formulations; 2012; Vol. 7.

(42) Gómez-Mingot, M.; Iniesta, J.; Montiel, V.; Kadara, R. O.; Banks, C. E. Direct Oxidation of Methionine at Screen Printed Graphite Macroelectrodes: Towards Rapid Sensing Platforms. *Sensors Actuators B Chem.* **2011**, *155* (2), 831–836.

(43) Mohamed, M. A.; El-Gendy, D. M.; Ahmed, N.; Banks, C. E.; Allam, N. K. 3D Spongy Graphene-Modified Screen-Printed Sensors for the Voltammetric Determination of the Narcotic Drug Codeine. *Biosens. Bioelectron.* **2018**, *101*, 90–95.

(44) Mohamed, M. A.; Atty, S. A.; Yehia, A. M.; Foster, C. W.; Banks, C. E.; Allam, N. K. Electrochemical Determination of the Serotonin Reuptake Inhibitor, Dapoxetine, Using Cesium–Gold Nanoparticles. *ACS Omega* **2017**, *2* (10), 6628–6635.

(45) Mohamed, M. A.; Atty, S. A.; Merey, H. A.; Fattah, T. A.; Foster, C. W.; Banks, C. E. Titanium Nanoparticles (TiO_2)/Graphene Oxide Nanosheets (GO): An Electrochemical Sensing Platform for the Sensitive and Simultaneous Determination of Benzocaine in the Presence of Antipyrine. *Analyst* **2017**, *142* (19), 3674–3679.

(46) Atty, S. A.; Mohamed, M. A.; Abd El Halim, L. M.; Fouad, F. A.; Boukherroub, R. Graphite/Nanocrystalline Zeolite Platform for Selective Electrochemical Determination of Hepatitis C Inhibitor Ledipasvir. *Electroanalysis* **2018**.

(47) Kamal Attia, A.; A. Mohamed, M.; M. Fekry, A. Electroanalytical Determination of Escitalopram Oxalate Using Nickel Nanoparticles Modified Carbon Paste Sensor. *Acta Chim. Slov.* **2017**, *64* (2), 415–421.

(48) Bandžuchová, L.; Šelešovská, R.; Navrátil, T.; Chýlková, J. Electrochemical Behavior of Folic Acid on Mercury Meniscus Modified Silver Solid Amalgam Electrode. *Electrochim. Acta* **2011**, *56* (5), 2411–2419.

Chapter 4

Experimental Methods and Materials*

4.1 Materials

All reagents were analytical grade and used as received without any further pre-treatments. TiO_2 nanoparticles (P25) and Graphite flakes (150µm flakes) were obtained from Sigma Aldrich, H_3PO_4, $K_3Fe(CN)_6$ and H_2SO_4 from Alfa Aesar, HCl, NaOH, CH_3COONa, and $KMnO_4$ from Loba Chemie, H_2O_2 from Fischer Scientific, CH_3COOH from Carlo Erba, paraffin oil used for pasting from Merck, and Hg standard solution (1000 ppm) from Agilent. For different pH values, 0.1 M acetate buffer solutions were prepared using different ratios of 0.1 M CH_3COONa and CH_3COOH solutions.

* Parts of this chapter were published in Abdullah, Ibrahim H., Nashaat Ahmed, Mona A. Mohamed, Fawzy MA Ragab, Marwa TA Abdel-Wareth, and Nageh K. Allam. "An engineered nanocomposite for sensitive and selective detection of mercury in environmental water samples." *Analytical Methods* 10, no. 21 (2018): 2526-2535.

And in Mohamed, Mona A., Menna M. Hasan, Ibrahim H. Abdullah, Ahmed M. Abdellah, Ali M. Yehia, Nashaat Ahmed, Walaa Abbas, and Nageh K. Allam. "Smart bi-metallic perovskite nanofibers as selective and reusable sensors of nano-level concentrations of non-steroidal anti-inflammatory drugs." *Talanta* 185 (2018): 344-351.

LOR was obtained from Novartis®, Egypt, with purity of 98.97%; PAR was generously supplied from CID CO®, Egypt, with purity of 99.34%. Pure graphite powder, bariam carbonate, niobium isopropoxide, ethanol absolute, and acetic acid were obtained from Sigma-Aldrich. Poly(vinylpyridine) (PVP, M.wt= 1,300,000) average Mw. Paraffin oil was obtained from Merck, and used as the binder liquid for preparing the pastes. Britton-Robinson buffer (B-R buffer) 40 mM was prepared by mixing boric acid, phosphoric acid, and acetic acid, then the solution was calibrated to pH values 2.0 - 9.0 using 0.2 M NaOH. Sterilized Milli-Q deionized water and analytical grade chemicals were used for all solution preparations.

4.2 Synthesis of Graphene Oxide

Graphene Oxide (GO) was prepared using Improved Hummer's method.[1] 3 g of graphite flakes were added to a mixture of H_3PO_4/H_2SO_4 (60:90 ml) and stirred in an ice bath till the temperature of -5 ^oC was reached. Then 18 g of $KMnO_4$ were added to the mixture in a slow rate to keep the temperature lower than 0 °C. This suspension was removed from the ice bath, raising its temperature to 50 °C, and then magnetically stirred for 24 h. The faint brown colored paste was then poured over a mixture of ice/water and allowed to stir for 15 min. A 20 ml of H_2O_2 was slowly added to quench the solution producing a yellow sol which was diluted with 1L of DI water and statically aged overnight. Then, the supernatant was removed away, and the solid material remained was washed several times with warm DI water and ethanol till the pH reached 6. Finally, the product was dried at 50 °C for 24 h.

4.3 Synthesis of RGO/TNT Nanocomposites

RGO/TNT nanocomposite was prepared through an alkaline hydrothermal method. A specific amount of GO was dispersed in 100 ml DI water by ultrasonic

stirring. Then 2 g of TiO_2 P25 (□25 nm) were suspended in the GO solution by ultrasonic stirring, followed by addition of 40 g NaOH and 1 h stirring. The mixture was transferred to a 200 ml-Teflon-lined autoclave and preserved at 160 ^oC for 23 h. The resultant gray precipitate was washed successively with distilled water, 0.1 M HCl, and distilled water until pH reached 7, then dried at 90 ^oC for 12 h. Finally, the collected product was calcinated in air at 300 ^oC (2 ^oC/min) for 10 h.[2]

4.4 Preparation of $BaNb_2O_6$ Nanofiber

Barium carbonate (1.0 g) was dissolved in acetic acid (3.0 g) and constantly stirred for 1 h at 70 °C till a clear solution of barium acetate was obtained. Then, a solution of 10 % PVP (MW = 1,300,000) in ethanol (99.9%) was prepared. Niobium isopropoxide (1.58 g) and barium acetate (4 g) solutions were slowly added to PVP solution (8 g) under continuous stirring to adjust the viscosity needed for electrospinning. Then, the spinning solution was used to fill a syringe with a fine metallic capillary needle. The solution was spun using a conventional electrospinning setup (MECC Nanon-01A, Japan) with a working distance of 15 cm, a working voltage of 26 kV, and a feeding rate of 3.9 ml /h. Samples were collected on aluminum foil, then dried and calcined for 4 h at 900 ^{0} C to obtain the final perovskite nanofiber.[3]

4.5 Instrumentation

Scanning electron microscopy (SEM) imaging was performed utilizing a Zeiss SEM Ultra 60 field emission scanning electron microscope (FESEM), equipped with Energy-dispersive X-ray spectroscopy (EDX). Images of High Resolution transmission electron microscopy (HRTEM) were obtained using a JEM-2010F electron microscope (JEOL, Japan), with accelerating voltage of 200 and 120 kV.

Fourier transform infrared spectroscopy (FTIR) measurements were carried out with a BRUKER Vertex 70 FTIR spectrometer. The phases and crystallinity were detected and identified using PANalytical (Empryan) 202964 X-Ray Diffractometer (XRD) using Cu Kα radiation (λ= 0.15406 nm) in the range of 5° to 80° at a scan rate (2θ) of 3^{o} s^{-1}. Raman measurements were performed by a Raman microscope (Pro Raman-L Analyzer) with an excitation laser beam wavelength of 532 nm. ICP-AES measurements were carried out by ICPE-9800 Series Simultaneous ICP Emission Spectrometer (Shimadzu, USA).

Voltammetric experiments were all performed utilizing CHI 760A Electrochemical Workstation (CH Instrument Inc., USA). As a counter electrode, a platinum wire (BAS, USA) was used, while Ag/AgCl (3.0 M NaCl) was employed as a reference electrode in respect to which all the electrochemical cell potentials were measured. All pH measurements were performed using a Cyberscan 500 digital (EUTECH Instruments, USA) pH-meter with a glass combination electrode. Electrochemical impedance spectroscopy (EIS) experiments were performed utilizing SP-150, Bio-Logic SAS and EC-Lab® software. The electrochemical measurements were all carried out at room temperature of 25±1 ^{o}C.

4.6 Preparation of Carbon Paste Electrodes (CPEs)

Using a glassy mortar, graphite powder (0.5 g) was mixed with paraffin oil (0.35 mL) to prepare the bare paste of CPE. Then, prepared paste was stuffed into the electrode hole whose surface was then made uniform using a filter paper till achieving a shiny appearance. For RGO/TNT/CPE preparation, the compound was mixed in different ratios with the graphitic unmodified paste using equivalent amounts of paraffin oil for 40 min to form uniformly and homogenously wetted modified pastes. For preparation of carbon paste electrode modified with $BaNb_2O_6$ ($BaNb_2O_6$/CPE),

three different amounts of $BaNb_2O_6$ nanofibers (50, 100 and 150 mg) were separately mixed well with graphite to obtain a total weight of 1000 mg nanocomposite. Each of the $BaNb_2O_6$/CPE pastes (5, 10 or 15 wt%) was utterly mixed with an adequate quantity of paraffin oil (0.35 mL) for 40 min, till obtaining a homogeneous and smooth wetted paste. The modified pastes were crammed in the electrode body the same way as the bare one.[4]

4.7 Experimental Conditions and Procedures

As for Hg(II) detection, a frequency range 100 mHz − 100 kHz was used to record all the impedance spectra. Cyclic voltammetry (CV) experiments were performed in a potential range between -300 to 750 mV vs. Ag/AgCl (3M NaCl) in which the scan rate was 100 mV s^{-1}. Under optimized conditions, square wave anodic stripping voltammetry (SWASV) was utilized to detect Hg^{2+} in different concentrations. Deposition of Hg was performed at a potential of -1.1 V for 180 s in which Hg^{2+} ions were reduced in presence of 0.1 M CH_3COONa/CH_3COOH (pH= 5.0). The anodic stripping, the process of oxidizing the electrodeposited metal from its atomic to ionic form, was carried out in a potential range between 0 and 0.45 V with the next parameters: increment potential, 4 mV; amplitude, 50 mV; frequency, 15 Hz. The real samples have been analyzed under the same electrochemical conditions. Before any electrochemical measurement were made, RGO/TNT was cycled in a range between 300 and 750 mV with scan rate of 100 mV s^{-1} in 0.1 M acetate buffer of pH 5 many times until a repeatable response was obtained. Then, the RGO/TNT-modified electrode was removed to a cell including the same buffer solution containing the proper amount of Hg(II) analyte. This has been applied for all other electrodes as well.[5]

For LOR detection, stock solutions of LOR and PAR (1.0 $x10^{-2}$ M) were prepared in ethanol and double distilled water, respectively. The essential amount of any of these stock solutions was transferred to a 5.0 mL standard volumetric flask, in which the solution volume was completed to the mark using $4.0x10^{-2}$ M Britton–Robinson buffer solution (pH 7.0). Prior to voltammetric measurements, the modified electrode ($BaNb_2O_6$/CPE) was cycled several times between 0 to +890 mV with a scan rate of 100 mV s^{-1} in B-R buffer of pH 7.0 till a reproducible behavior was obtained. Then, $BaNb_2O_6$/CPE electrode was placed in to a different cell containing a proper amount of LOR in B-R buffer of pH 7.0. Cyclic voltammograms were recorded using the same parameters.[6]

For SWASV measurements, aliquots with LOR concentrations from 5.0×10^{-8} to 1.4×10^{-4} M were moved to a series of 5.0 mL volumetric flasks using micropipette. The volume was then diluted to reach the 5-ml flask mark by adding B-R buffer pH 7.0. By transferring 5 ml of the solution to the electrolytic cell, SWV was made ready to record. A scan rate of 40 mVs^{-1} was used to detect the current response of SWV measurements at the $BaNb_2O_6$/CPE working electrode. Also, the pulse period during chronoamperometry was 30 s while the impedance measurements were performed over a frequency range of 100 mHz − 100 kHz.

4.8 Real Polluted Water Samples Preparation

The water samples were collected from three different polluted sites in Qarun lake, Egypt, where many industrial plants are in operation around. The samples were pretreated by filtration, using 0.2 μm membrane to eliminate suspended particles and other organic impurities. Then, all samples were adjusted to pH 5.0 using 0.1 M acetate buffer. The Hg(II) concentration in the pretreated samples was then analyzed

using both inductive coupled plasma atomic emission spectrometry (ICP-AES) and the fabricated sensing platform.[7]

4.9 Spiked Plasma Samples Preparation

Immediately prior to the experimental measuring, plasma samples were drawn from a healthy individual, in which 0.5 mL of the sample was injected into a 5-mL volumetric flask spiked with 1.0×10^{-3} M of LOR standard solution of different volumes, containing B-R buffer (pH 7). Then, the solution was directly moved to the voltammetric cell for analysis. The experimental measurements were all carried out in accordance with the institutional guidelines and conventional laws, after having the approval of the institutional ethics committees.

4.10 References

(1) Marcano, D. C.; Kosynkin, D. V.; Berlin, J. M.; Sinitskii, A.; Sun, Z.; Slesarev, A.; Alemany, L. B.; Lu, W.; Tour, J. M. Improved Synthesis of Graphene Oxide. *ACS Nano* **2010**, *4* (8), 4806–4814.

(2) Liu, N.; Chen, X.; Zhang, J.; Schwank, J. W. A Review on TiO2-Based Nanotubes Synthesized via Hydrothermal Method: Formation Mechanism, Structure Modification, and Photocatalytic Applications. *Catal. Today* **2014**, *225*, 34–51.

(3) Hildebrandt, N. C.; Soldat, J.; Marschall, R. Layered Perovskite Nanofibers via Electrospinning for Overall Water Splitting. *Small* **2015**, *11* (17), 2051–2057.

(4) Mohamed, M. A.; Atty, S. A.; Merey, H. A.; Fattah, T. A.; Foster, C. W.; Banks, C. E. Titanium Nanoparticles (TiO_2)/Graphene Oxide Nanosheets (GO): An Electrochemical Sensing Platform for the Sensitive and Simultaneous Determination of Benzocaine in the Presence of Antipyrine. *Analyst* **2017**, *142* (19), 3674–3679.

(5) Kamal Attia, A.; A. Mohamed, M.; M. Fekry, A. Electroanalytical Determination of Escitalopram Oxalate Using Nickel Nanoparticles Modified Carbon Paste Sensor. *Acta Chim. Slov.* **2017**, *64* (2), 415–421.

(6) Atty, S. A.; Mohamed, M. A.; Abd El Halim, L. M.; Fouad, F. A.; Boukherroub, R. Graphite/Nanocrystalline Zeolite Platform for Selective Electrochemical Determination of Hepatitis C Inhibitor Ledipasvir. *Electroanalysis*. John Wiley & Sons, Ltd September 24, 2018.

(7) Bagheri, H.; Afkhami, A.; Khoshsafar, H.; Rezaei, M.; Sabounchei, S. J.; Sarlakifar, M. Simultaneous Electrochemical Sensing of Thallium, Lead and Mercury Using a Novel Ionic Liquid/Graphene Modified Electrode. *Anal. Chim. Acta* **2015**, *870*, 56–66.

Chapter 5

Results and Discussion[†]

5.1 RGO/TNT as an Electrochemical Modifier for Hg(II) Sensing

5.1.1 Morphological and Structural Characterization of RGO/TNT Nanocomposite

Intercalating the TiO_2 nanotubes between the sheets of graphene helps to boost the amount of Hg(II) adsorbed on the electrode surface. This distinctive structure is also important to diminish the probability of graphene sheets to agglomerate. Figure 5-1a, b shows the FESEM and HRTEM images of the fabricated pure GO sheets, respectively. Note that very thin free-standing graphene sheets, with micrometer scale dimensions both in width and length, entail a considerable degree of crumbling, which would enhance their electronic and chemical properties.[1] The FESEM image in Figure 5-1c shows how the TiO_2 one-dimensional structures are attached to the RGO sheets in the composite, helping to keep them separate. Also, Figure 5-1d depicts the TEM image of RGO/TNT nanocomposite clarifying that TNT has one-dimensional tubular morphology with an average diameter of 10±0.8 nm and a length of 100-200 nm, being spread all over the RGO sheets. The flake morphology of RGO can be also identified due to its typical sheet-like structure and sheet edges shape.

[†] Parts of this chapter were published in Abdullah, Ibrahim H., Nashaat Ahmed, Mona A. Mohamed, Fawzy MA Ragab, Marwa TA Abdel-Wareth, and Nageh K. Allam. "An engineered nanocomposite for sensitive and selective detection of mercury in environmental water samples." *Analytical Methods* 10, no. 21 (2018): 2526-2535.

And in Mohamed, Mona A., Menna M. Hasan, Ibrahim H. Abdullah, Ahmed M. Abdellah, Ali M. Yehia, Nashaat Ahmed, Walaa Abbas, and Nageh K. Allam. "Smart bi-metallic perovskite nanofibers as selective and reusable sensors of nano-level concentrations of non-steroidal anti-inflammatory drugs." *Talanta* 185 (2018): 344-351.

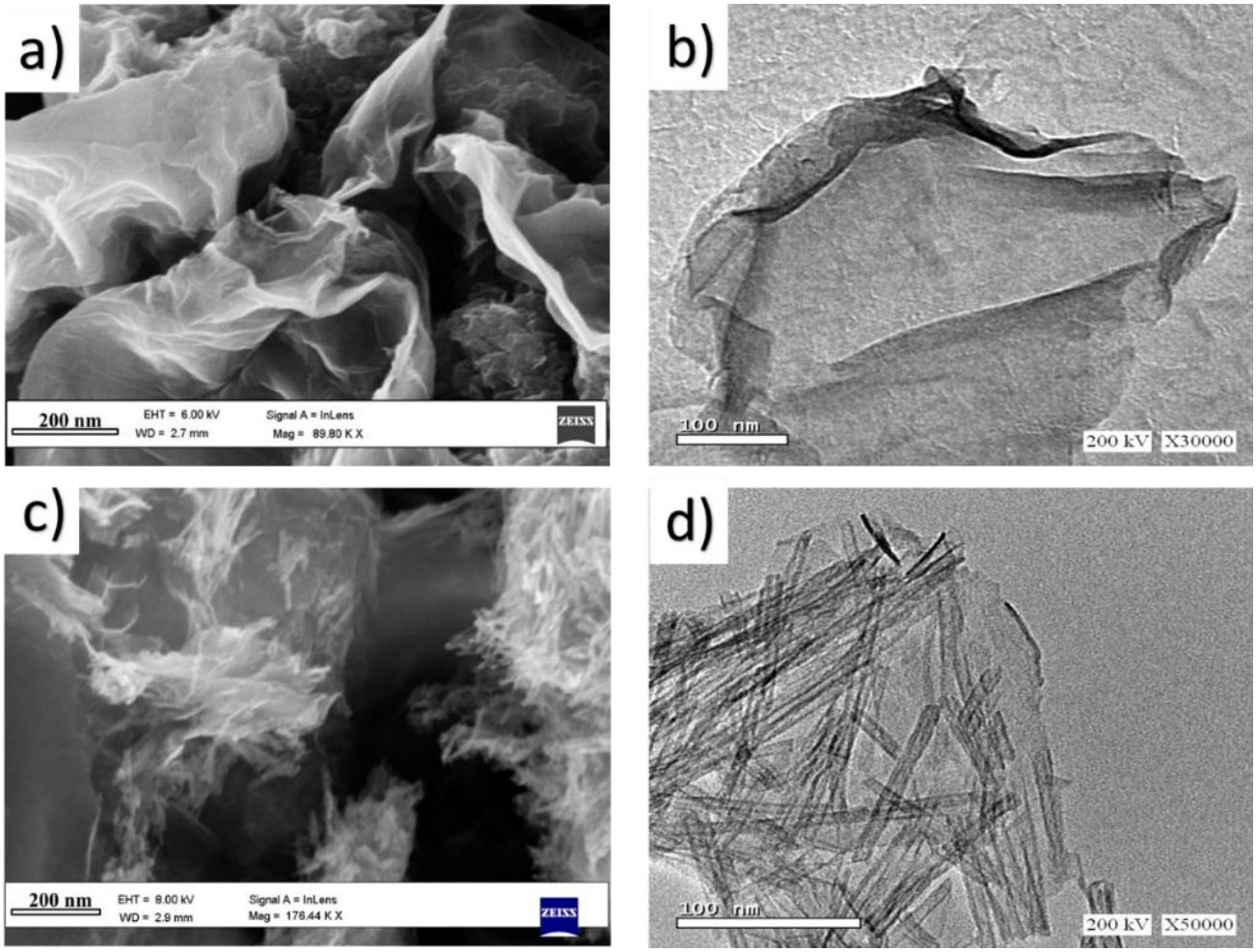

Figure 5-1. (a) FESEM, (b) HRTEM images of the pristine GO, along with (c) FESEM, and (d) HRTEM images of the prepared RGO/TNT nanocomposite.

To understand the interaction between RGO and TNTs, Fourier-transform infrared (FTIR) spectroscopy was performed, Figure 5-2a. The FTIR spectrum of GO shows a broad peak at 3400 cm^{-1}, which is ascribed to the stretching vibration of hydroxyl groups (–OH). Other multi-peaks are also related to oxygen-containing functional groups such as carboxylates (−C−O−) (1051 cm^{-1}), epoxide (−C−O−C−) (1370 cm^{-1}), and ketenes (−C=O) (1729 cm^{-1}). [2,3]The broad band at 1616 cm^{-1} can be ascribed to in-plane vibrations of aromatic C=C sp^2 hybridized carbons.[4] On the other hand, the FTIR spectrum of RGO/TNT shows low frequency bands around 496 cm^{-1} and 738 cm^{-1} related to Ti−O−Ti and Ti−O−C, respectively, due to the chemical interaction of RGO with the TNTs.[5] Also, the decrease in the oxygen-containing

functional groups has been observed, demonstrating that GO was significantly reduced by the hydrothermal treatment, which promotes the hybridization of TNTs deposited on the RGO sheets.[3]

Figure 5-2b shows the XRD patterns of GO and RGO/TNTs composite. The GO spectrum exhibits one characteristic diffraction peak at 2θ = 10.9° corresponding to the plane (002), having an interlayer distance of ~0.86 nm, which is larger than that of graphite (~0.33 nm).[6] The large expansion of d-spacing of GO compared to graphite is usually ascribed to the insertion of oxygen containing groups and H_2O molecules.[7] The XRD pattern of RGO/TNTs (top in Figure 5-2b) showed peaks at 25.35°, 37.92°, 44.67°, 54.23°, 62.68°, 69.2°, 75.08°, which are related to (101), (004), (200), (105), (211), (204), (116), (220), and (215) plans, respectively. These planes corresponded to the anatase crystalline phase (ICDD Card no: 00-021-1272). It has been noticed that the distinctive peak for GO disappeared in the composite pattern, which is due to the conversion of GO into RGO under alkaline hydrothermal conditions.[8] Nonetheless, the characteristic peaks related to RGO were not noticed because the peak of (101) plane of anatase appears at almost the same 2θ value, especially that the percentage of RGO in the composite is lower than the detection limit of XRD.[9] Based on the XRD peak broadening of the (101) peak, the average crystallite size (D) and micro strain (ε_{str}) of the TNTs and RGO/TNTs were calculated to be 7.7 nm and 2.255%, respectively, using Scherrer's (Eq. 5.1) and Wilson's equations (Eq. 5.2).[9]

$$D = k.\lambda/\beta.cos\theta \qquad (5.1)$$

$$\varepsilon_{str} = \beta/4\tan\theta \quad (5.2)$$

where β is the full width at half maximum (FWHM) intensity, k is the shape factor (0.90), λ is the incident X-ray wavelength, and θ is Bragg's angle.

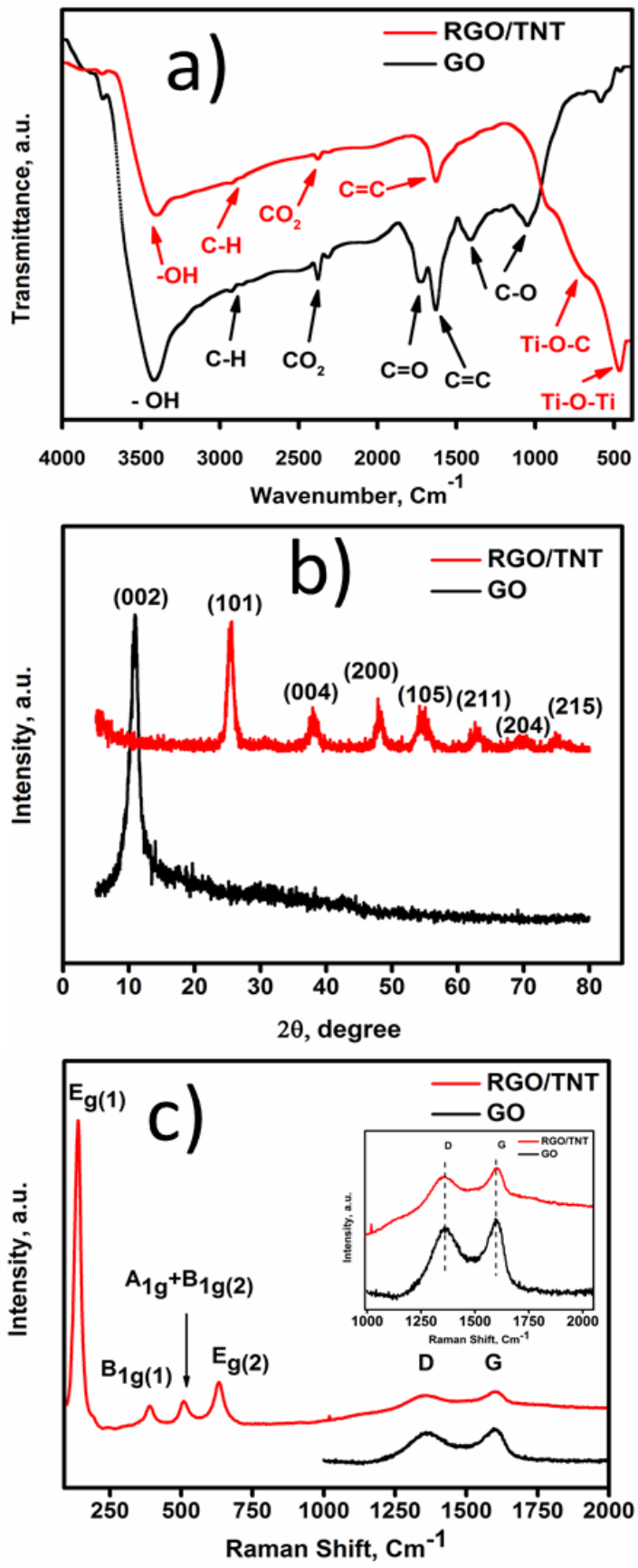

Figure 5-2. (a) FTIR, (b) XRD, and (c) Raman spectra of both pristine GO and RGO/TNT; the inset in c shows the shift in D and G Raman bands.

The Raman spectra of the GO and RGO/TNT are shown in Figure 5-2c. The prominent bands at 1343 and 1597 cm^{-1} are corresponding to the D and G bands of the GO sample, respectively. The D band corresponds to the ring breathing modes of sp^2 carbon atoms that are adjacent to a defect or an edge, while the G band to sp^2 carbon atoms in a planar and conjugated structure. The low ratio of D to G bands (I_D/I_G) can be attributed to a low concentration of defects and disorders in the graphitized structures.[10] Also, Raman spectra confirmed the formation of RGO/TNTs composite in which several characteristic Raman peaks at 141, 390, 512 and 635.46 cm^{-1} were obtained, corresponding to the $E_{g(1)}$, $B_{1g(1)}$, A_{1g} with $B_{1g(2)}$, and $E_{g(2)}$ modes of anatase TNTs, respectively. No peaks corresponding to rutile or brookite phases were observed, which is consistent with the XRD results. The D band (1334 cm^{-1}) and G band (1602 cm^{-1}) of the RGO/TNTs sample were, respectively, red and blue-shifted (Figure 5-2c inset) compared to those of the GO, which is attributed to the reduction of GO into RGO. Also, it may be due to a change of surface pressure after adsorption on TNTs surface.[10,11]

5.1.2 Electrochemical Characterization of RGO/TNT Nanocomposite

Cyclic voltammetry (CV) was utilized to investigate the electrochemical behavior of different bare and modified CPEs using the redox couple of $[Fe(CN)_6]^{3-/4-}$ in a solution of 1.0 mM $[Fe(CN)_6]^{3-/4-}$ and 0.1 M KCl. Figure 5-3a reveals the relatively weak redox current of the bare CPE (black curve) with a peak-to-peak separation potential ($\Delta E_p = E_{pa} - E_{pc}$) of 380 mV, indicating a sluggish electron transfer process and low electrical conductivity.[12] TNTs-modified CPE (green curve) shows a slightly increasing redox current response with a narrower ΔE_p (269 mV) than that of graphitic CPE, indicating a relatively better electron transfer kinetics, which can be ascribed to the one-dimensional tubular structure of TiO_2 that may lead

to better charge collection.[13] Higher values of both anodic and cathodic currents were demonstrated by the RGO-modified CPE (red curve), which could be attributed to its zero band gap electronic structure and considerable 2-D electrical conductivity.[14] Upon modifying the CPE with RGO/TNTs, the redox current significantly increased to ~ 1.45 times that of RGO-modified CPE. Also, the ΔE_p value was the lowest (179 mV) among the other electrodes, indicating high rate of electron transfer process and better reaction reversibility at the electrode surface.[15] This reveals that the synergetic effect of involving both RGO and TNTs in the modified paste might provide the required conduction pathway for the electrocatalytic detection mechanism. This behavior may be attributed to the edge plane defects that open up during the hydrothermal process, leading to notably higher surface area and more facile electron transfer kinetics in the resulting nanocomposite.[16]

EIS is a vital technique to investigate the feasibility of the charge transfer process across the electrode surface as well as the kinetics and mass transport parameters. Figure 5-3b shows the EIS plots of different CPEs that are both bare and TNT, RGO, and RGO/TNTs-modified, in which the measurements were carried out using 1.0 mM $[Fe(CN)_6]^{3-/4-}$ containing 0.1 M KCl. The high frequency region verified a semicircle behavior is corresponding to the charge transfer resistance at the electrode surface. The obtained Nyquist plots for the different electrodes have revealed a Warburg-type equivalent circuit model, which is shown in the inset of Figure 5-3b. Qualitatively, the charge transfer is enhanced using TNTs, RGO, RGO/TNTs-modified CPEs as compared to the unmodified counterpart, as indicated *via* the radii of the semicircles. The value of charge transfer resistance (R_{ct}) was found to be 3634 Ω and 2223 Ω for bare CPE and TNTs-modified CPE, respectively, which might be owing to the large surface area of TiO_2 one-dimensional structure in which

the inner layer behavior of the porous structure can facilitate the diffusion.[17] Also, the RGO-modified CPE showed an even lower resistance (1436 Ω), which can be attributed to the superior conductivity of graphene. The R_{ct} value was decreased to 817.7 Ω in the case of RGO/TNTs-modified CPE, demonstrating an improved reaction reversibility at the electrode surface.

Furthermore, Figure 5-3c presents the SWASV measurements recorded for bare, TNTs, RGO, and RGO/TNTs-modified CPEs. With an accumulation process performed for 180 s at a potential of -1.1 V in a solution of 1.0 μM Hg(II) containing 0.1 M acetate buffer (pH 5.0), almost no peak was detected using bare CPE (black line) in the potential range of 0 − 0.45 V. However, a weak and wide peak was observed at the TNTs-modified CPE (green line) and a higher one was found with RGO-modified CPE (red line). Although it might have been expected to obtain intense peaks using pure graphene oxide instead of RGO due to the anchor sites provided by its many functional groups, it was found that desorbing the Hg ions from the electrode surface was very difficult, which would affect the reusability of the electrode. The sharpest and highest peak current (at a potential of 0.24 V) was demonstrated by the RGO/TNTs-modified CPE, which indicates a proper accumulation of Hg(II) on the electrode surface yielding an enhanced sensitivity.[18] These findings are consistent with those of the CV and EIS measurements, indicating that RGO/TNTs nanocomposite can provide better electrical conductive pathways as a CPE modifier owing to the synergistic influence of its components.

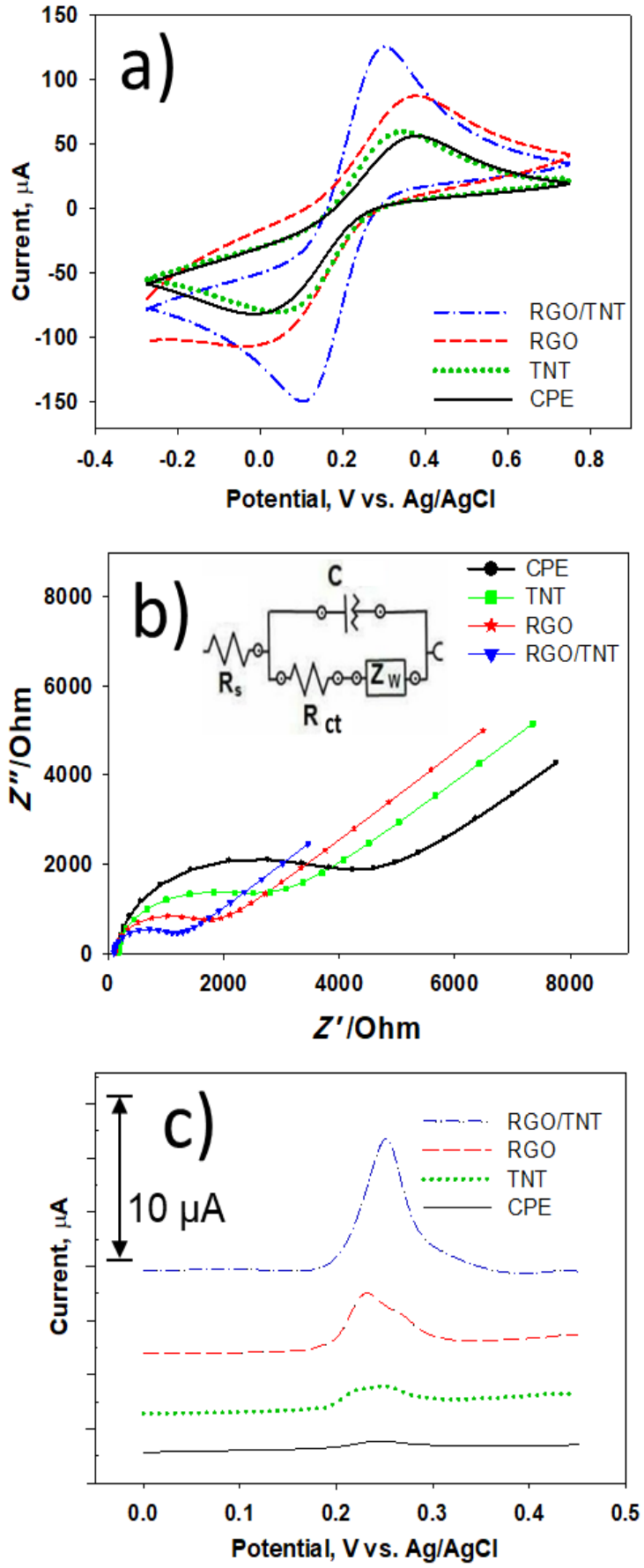

Figure 5-3. (a) Cyclic voltammograms of bare CPE along with TNT, RGO, and RGO/TNT-modified CPEs in a solution of 1.0 mM $[Fe(CN)_6]^{3-/4-}$ and 0.1 M KCl with a scan rate of 100 mV s^{-1}. (b) EIS plots for both the modified and unmodified CPEs in 1.0 mM $[Fe(CN)_6]$. (c) SWASV of all electrodes against a solution of 1µM Hg(II).

5.1.3 Interaction Between TNT and Hg (II) Ions

TiO_2 nanotubes act as a supporting constituent in the fabricated composite. Its tubular structure helped to increase the probability of Hg (II) ions on its high surface area. Through their very thin walls, TiO_2 nanotubes significantly facilitated the charge carrier movement to be collected from the Hg (II) ions. Typically, the ions have various possibilities either to attach to nanotubular nozzles or themselves embed into the tubes or between the tubes and RGO sheets. Some even may disperse inside the tubes, to be adsorbed on the inner tubular walls or enwrapped on the tubes mouth. TiO_2 nanotubes also helped to act as scaffold for the reduced graphene oxide sheets whose conductive properties were a main player to boost the electrochemical activity of the whole nanocomposite. This explanation is reinforced by the electrical behavior both TNT and TNT/RGO composite showed in both the CV and EIS measurements.

5.1.4 Optimization of the Experimental Conditions

To obtain the highest possible sensitivity toward the trace Hg^{2+} concentration using RGO/TNTs-modified CPE, a series of experiments was conducted to determine the influence of the various voltammetric parameters involved in SWV. The effects of pH, deposition potential, and deposition time were investigated in a solution containing 1.0 μM of Hg(II). The influence of operating temperature was not considered as Hg^{2+} was designed to work at the ambient temperature. It is essential to study how the value of pH of the environmental samples affects the Hg^{2+} sensor. Figure 5-4a depicts the effect of a range of pH values from 3.0 to 6.0 on the voltammetric current response using acetate buffer solution (0.1 M). The corresponding current in SWV changed with different pH values from 3.0 to 5.0, where it reached the maximum value. This may be owing to the mechanism of electrostatic attraction and complexation, in which the carboxylic and hydroxyl

groups can act as anchor sites to absorb Hg ions.[14] Then, the stripping signal has slightly declined after 5.0 to 6.0, which may be related to the hydrolysis of Hg ions. Consequently, 0.1 M acetate buffer solution with pH 5.0 was selected to conduct the SWV measurements.

In stripping voltammetry, it is essential to select an adequate deposition potential in order to achieve the highest possible sensitivity. Hence, at pH 5.0 and after accumulation time of 180 s, the effect of deposition potential on the current response was investigated. The results clarifying how a range of deposition potentials from -0.5 to -1.1 V affected the value of the signal response are presented in Figure 5-4b. It was found that the more negative the deposition potential was, the higher the peak current values obtained from Hg(II) ions. Although it was expected for values more negative than -1.1 V to exhibit higher signal response, a value of -1.1 V was chosen as an optimum deposition potential for the conducted experiments to evade both the other metal ions codeposition in real environmental samples and the competitive generation of H_2 gas that is more likely to happen after a potential of -

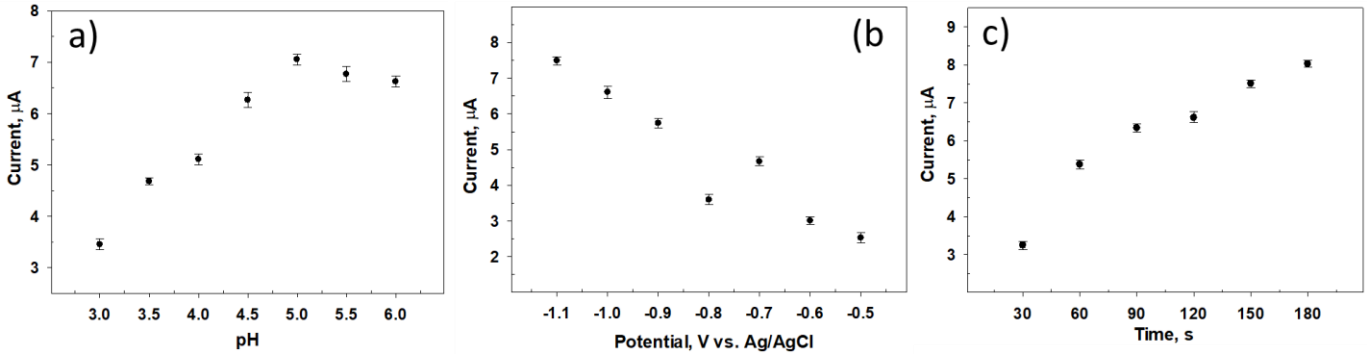

Figure 5-4. Optimization of the effect of the voltammetric parameters of (a) pH, (b) Deposition potential, and (c) Deposition time on the current response of RGO/TNT nanocomposite-modified CPE. Measurements were recorded by SWASV of 1.0 µM of Hg(II) solutions.

1.23 V vs. NHE.

Additionally, it is important to study the effect of deposition time on the stripping measurements as it can enhance the sensitivity and detection limit of the

sensor. Figure 5-4c describes the dependence of the obtained current on the deposition time, in a range between 30 to 180 s. As demonstrated, the achieved peak current increased as the deposition time was extended to 180 s, which is attributed to the increased amount of analyte ions absorbed on the electrode surface. While more deposition time is suggested to show better sensitivity, it also can decrease the upper detection limit as the electrode surface becomes saturated when metal ion concentration is high.[51] Thus, to achieve more sensitive behavior with a broad detection range, deposition potential of 180 s was chosen for the subsequent experiments.

5.1.5 Stripping Response Toward Hg(II)

Under the optimized experimental conditions, SWASV was employed to determine the analytical behavior of RGO/TNTs-modified CPE toward different concentrations of Hg(II), Figure 5-5a. Well-defined peak currents corresponding to the electrochemical oxidation of Hg were obtained using RGO/TNTs-modified CPE as a sensing platform. The peak current values (I) were found to be linearly proportional to Hg(II) concentrations (C) over a range from 2.5×10^{-10} M to 5×10^{-6} M with a linearization equation: $I/\mu A = 6.280\ C/\mu M + 0.768$; $R^2 = 0.9992$. The equation LOD = 3S/x was employed to calculate the LOD, where S is the standard deviation of the current response (n=5) and x is the slope of the calibration curve (see Figure 5-5b). The LOD was calculated to be 4×10^{-11} M. This limit is much lower than the permissible limits of Hg concentrations given by both WHO and the U.S. EPA. The results obtained are represented in Table 5-1, proving to be comparable to many of the recently reported studies,[19,20] in which the proposed non-enzymatic, mobilized, and label-free sensing platform utilizes cost-effective materials with facile fabrication procedures.

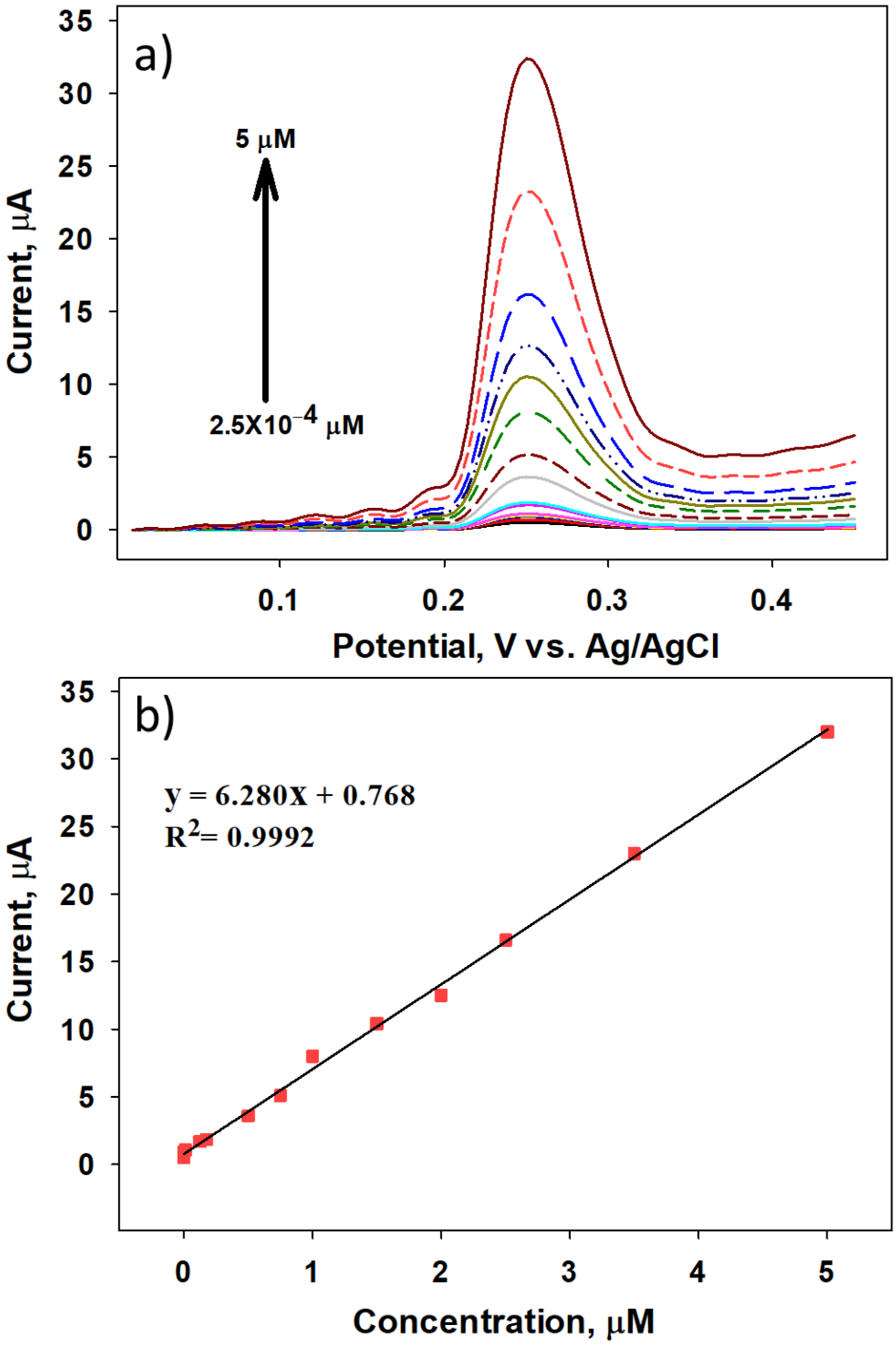

Figure 5-5. (a) SWASV graphs resulted using of RGO/TNT-modified CPE to detect Hg(II) over a concentration ranging from 2.5×10^{-4} μM to 5 μM in 0.1 M acetate buffer (pH 5) with scan rate of 100 mV s^{-1}. (b) The calibration curve resulted by plotting the peak response.

Table 5-1: Comparison between some electrochemical sensors reported to detect Hg(II).

Materials	Linear ranges (M)	LOD (M)	Ref.
Au/Nafion/GCE	$25\times10^{-9} - 225\times10^{-9}$	18.9×10^{-9}	[19]
ZnO QDs	$25\times10^{-9} - 250\times10^{-6}$	25×10^{-9}	[21]
Gr-DNA based	$8\times10^{-9} - 1\times10^{-7}$	5×10^{-9}	[22]
SWCNT/PhSH/Au	$5\times10^{-9} - 9\times10^{-8}$	3×10^{-9}	[23]
Au-DNA based	$1\times10^{-10} - 1\times10^{-7}$	3×10^{-11}	[20]
IL/Gr/L/CPE	$1.25\times10^{-9} - 2\times10^{-7}$	3.57×10^{-10}	[15]
C_3N_4/Chitosan	$1\times10^{-7} - 5\times10^{-6}$ and $1\times10^{-6} - 8\times10^{-5}$	1×10^{-8}	[24]
RGO/TNT/CPE	$2.5\times10^{-10} - 5\times10^{-6}$	4×10^{-11}	This work

5.1.6 Simultaneous Detection of Hg(II), Cu(II), and Mn(II)

Fertilizers and pesticides frequently contain ions of Hg, Pb, Cu, As, Mn, and Fe.[18] During irrigation process, these ions are transferred to the soil and main water streams acting as permanent pollutants. Some of these ions may interfere with Hg(II) detection process such as Cu(II), which forms Cu-Hg intermetallic bonds shielding the Hg ions from the redox process at the electrode surface, especially at low concentrations.[14] Thus, to examine the specificity of the proposed sensing platform toward Hg(II), its electroanalytical behavior was simultaneously observed in presence of Cu(II) and Mn(II). As shown in Figure 5-6a, the SWASV graphs obtained during the simultaneous detection of Hg(II) with Cu(II) and Mn(II) show three separate anodic peaks at potentials of 0.24, -0.12, and 0.8 V, respectively, representing the feasibility of detecting these ions simultaneously using our RGO/TNTs-modified CPE. The measurements were performed under the above-mentioned optimized conditions over a range of concentrations from 5×10^{-9} to 3×10^{-6} M; scan rate, 100 mV

s^{-1}. Figure 5-6b displays the calibration curve in which the peak current of each of the metals is plotted against its various concentrations. As demonstrated, linear relations were found to be applicable within the above-mentioned concentration range with regression equations of I/μA = 5.833 C/μM + 0.774; R^2 = 0.9989, I/μA = 3.779 C/μM + 0.489; R^2 = 0.9991, and I/μA = 2.478 C/μM + 0.323; R^2 = 0.9994, for Hg(II), Cu(II), and Mn(II), respectively.

Accordingly, the sensitivity of the RGO/TNTs-modified CPE toward Hg(II) was found to be 5.833 μA/μM, which is quite close to that obtained in the absence of Cu(II) and Mn(II) (6.280 μA/μM). This designates that oxidation processes of these different heavy metal ions at the surface of the proposed sensing platform are almost independent and thus, their simultaneous detection is feasible with low probability of remarkable interference. Using the equation LOD = 3S/x, the LOD of Hg(II) in these

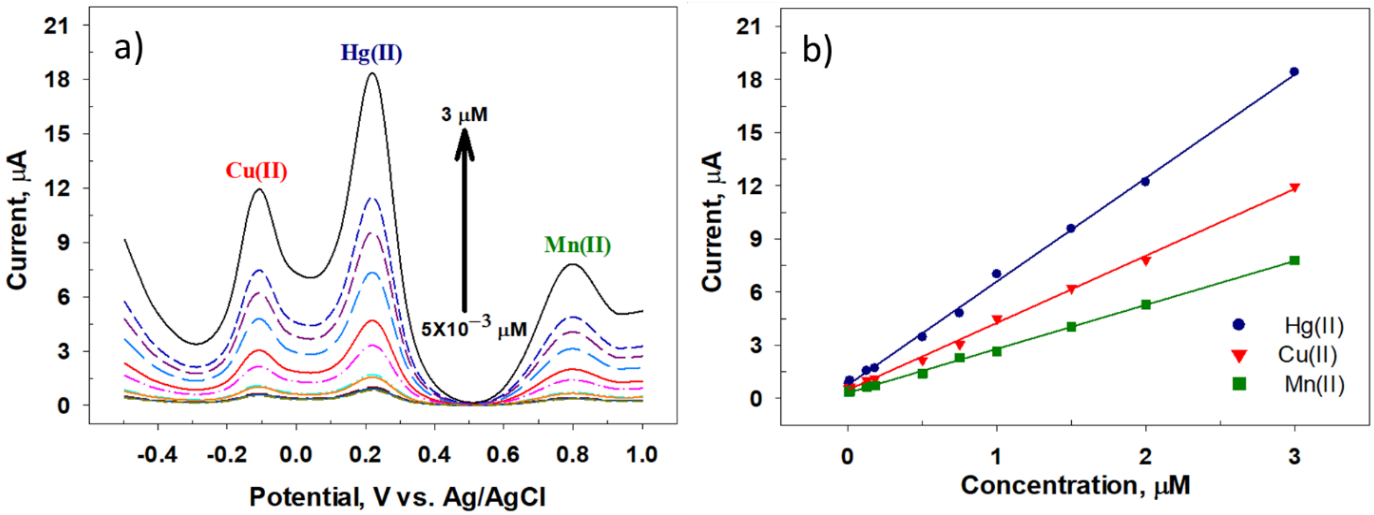

Figure 5-6 (a) SWASV graphs using of RGO/TNT-modified CPE in 0.1 M acetate buffer solution (pH 5.0) containing different concentrations of Hg(II), Cu(II), and Mn(II) from 5×10^{-9} to 3×10^{-6} M; scan rate, 100 mV. (b) Calibration curve of each heavy metal in the simultaneous detection process, plotting the resulting peak current as a function of the metal ions concentration ranging from 5×10^{-9} to 3×10^{-6} M.

simultaneous measurements was calculated to be 8×10^{-10} M.

5.1.7 Interference Study of Adjacent Heavy Metal Ions

Under the optimized conditions, the current density resulting from voltammetric current measurements of Hg^{2+} were recorded in presence of a variety of interfering ions. In addition to Cu^{2+} and Mn^{2+}, ions like Na^{+}, K^{+}, Ca^{2+}, and Mg^{2+} were injected to test the sensor's response. The experiments were performed using solutions of 1.0 μM Hg(II) containing 0.1 M acetate buffer (pH 5.0), in presence of the interfering ions of the same concentration each. As shown in Figure 5-7, the current readings showed almost consistent behavior, which is due to the high specificity of the sensor towards Hg^{2+} ions. The most noticeable negative fluctuation of the current was in presence of Cu^{2+} ions. This may be attributed to the Hg−Cu intermetallic bonds that can produce a misleading effect in the signaling current.

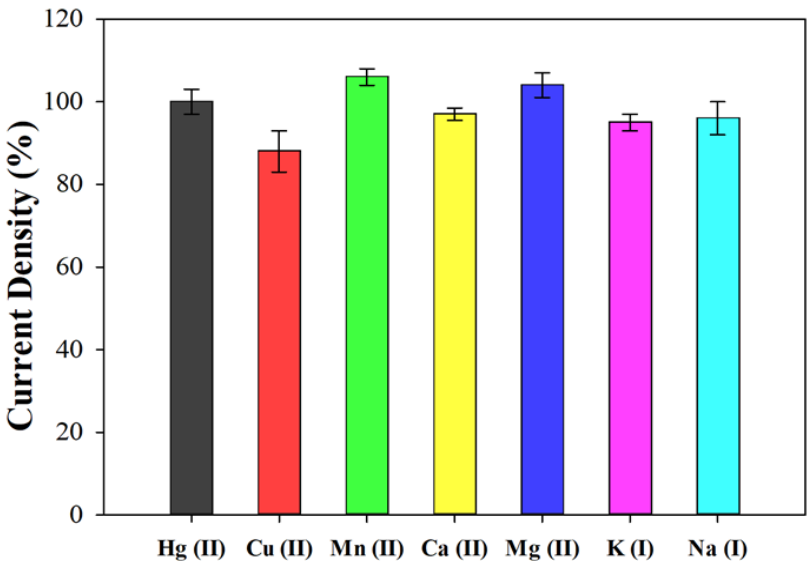

Almost all the other ions did not affect the current response in such a way. This probably maybe ascribed to the fingerprint potential values of these ions that are relatively far from that of mercury.

Stability Measurements

Figure 5-8 shows the stability and repeatability test of the RGO/TNTs-modified CPE over 25 runs against 1.0 μM Hg(II) in 0.1 M acetate buffer solution

Figure 5-7 Interfering effect of various heavy metal ions against the volumetric detection measurements of Hg^{2+}ions.

(pH 5.0). The peak currents of the SWASV measurements obtained using the proposed CPE modifier were reproducible with a relative standard deviation (RDS) of 0.928%. The results reveal that RGO/TNTs-modified CPE exhibits an outstanding

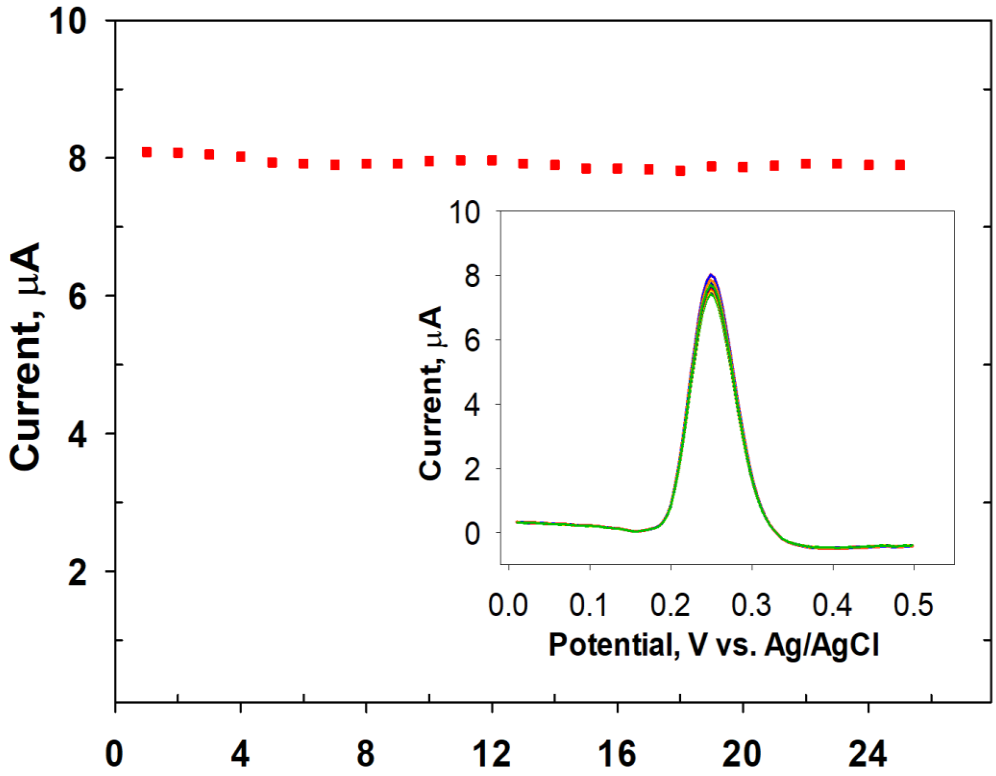

Figure 5-8 SWASV recorded peak currents of 1.0 µM Hg(II) on RGO/TNT-modified CPE sensing platform in 0.1 M acetate buffer (pH 5.0); scan rate, 100 mV s^{-1}. The inset displays the corresponding obtained plots from the stripping measurements over 25 runs.

reproducibility and stability under the repeated analytical measurements, using the optimized experimental conditions.

5.1.8 Real Polluted Water Sample Analysis

To verify the practicality of the fabricated sensor, it was tested to detect Hg(II) in real environmental water samples. After pretreatment, the presence of Hg(II) was investigated in the samples using both the proposed sensing platform and ICP-AES. Hg(II) was not detected in two of the three samples. Then, they were all spiked with 5×10^{-8} M Hg(II). Clearly, highly consistent results were obtained from ICP-AES and our sensor (see Table 5-2). Moreover, compared to ICP-AES, the sensor overcame

some shortcomings such as expensive equipment, tedious sample preparation, and reagent consumption. Accordingly, RGO/TNTs-modified CPE showed a significant potential to be reliable for real water samples.

Table 5-2: Results of Hg(II) determination in real water samples.

#	Added ($\times10^{-8}$ M)	Found ($\times10^{-8}$ M)	Recovery (%)	ICP-AES
1	0.00	ND[a]	–	ND
	5.00	4.97 (±0.16)	99.4	5.13 (±25)
2	0.00	ND	–	ND
	5.00	5.06 (±0.21)	101.2	5.21 (±0.32)
3	0.00	42.54 (±0.13)	–	42.72 (0.26)
	5.00	47.78 (±0.22)	100.5	47.95 (±0.41)

[a] ND, not detected.
Values between parentheses are S.D. of three replicate measurements.

5.2 $BaNb_2O_6$ Nanofibers as an Electrochemical Modifier for LOR Sensing

5.2.1 Morphological and Structural Characterization of $BaNb_2O_6$ Nanofibers

The morphology of the developed modifier was investigated using SEM imaging, Figure 5-9. The nanofibers, in general, exhibit well-defined morphology, with fibers diameters ranging from tens to hundreds of nanometers, which could be further adjusted according to the targeted application via controlling several parameters such as polymer concentration, solvent type, and spinning conditions. Figure 5-9B, C reveals that the obtained morphology has been maintained even after being annealed at high temperature, where the nanofibers are composed of small plate-like crystallites. The EDX analysis shows the presence of Ba, Nb, and O elements, which confirms the composition of the fabricated nanofibers, Figure 5-9D.

The successful formation of $BaNb_2O_6$ nanofibers was further confirmed using

powder x-ray diffraction (PXRD) (Figure 5-10). The PXRD patterns of $BaNb_2O_6$

strongly proved the orthorhombic crystal structure of the resulted nanofibers, in

accordance with (JCPDS: 14–27). In addition, the prepared nanofibers were

characterized by HRTEM after calcination at 950 °C, Figure 5-11. The HRTEM

images shown in Figure 5-11 indicate that the nanofibers are essentially composed of

intergrown single crystals.[25,26] A lattice fringe spacing of 0.2991 nm was observed,

which corresponds to (023) plane of the fabricated nanofibers, exhibiting

orthorhombic structure. This is supporting to the results obtained by PXRD

measurements. Also, the presence of single crystals as the building blocks of the

fibers can be further verified by the bright spots of the selected area electron diffraction (SAED) pattern. The occurring double-spots in SAED occur from several

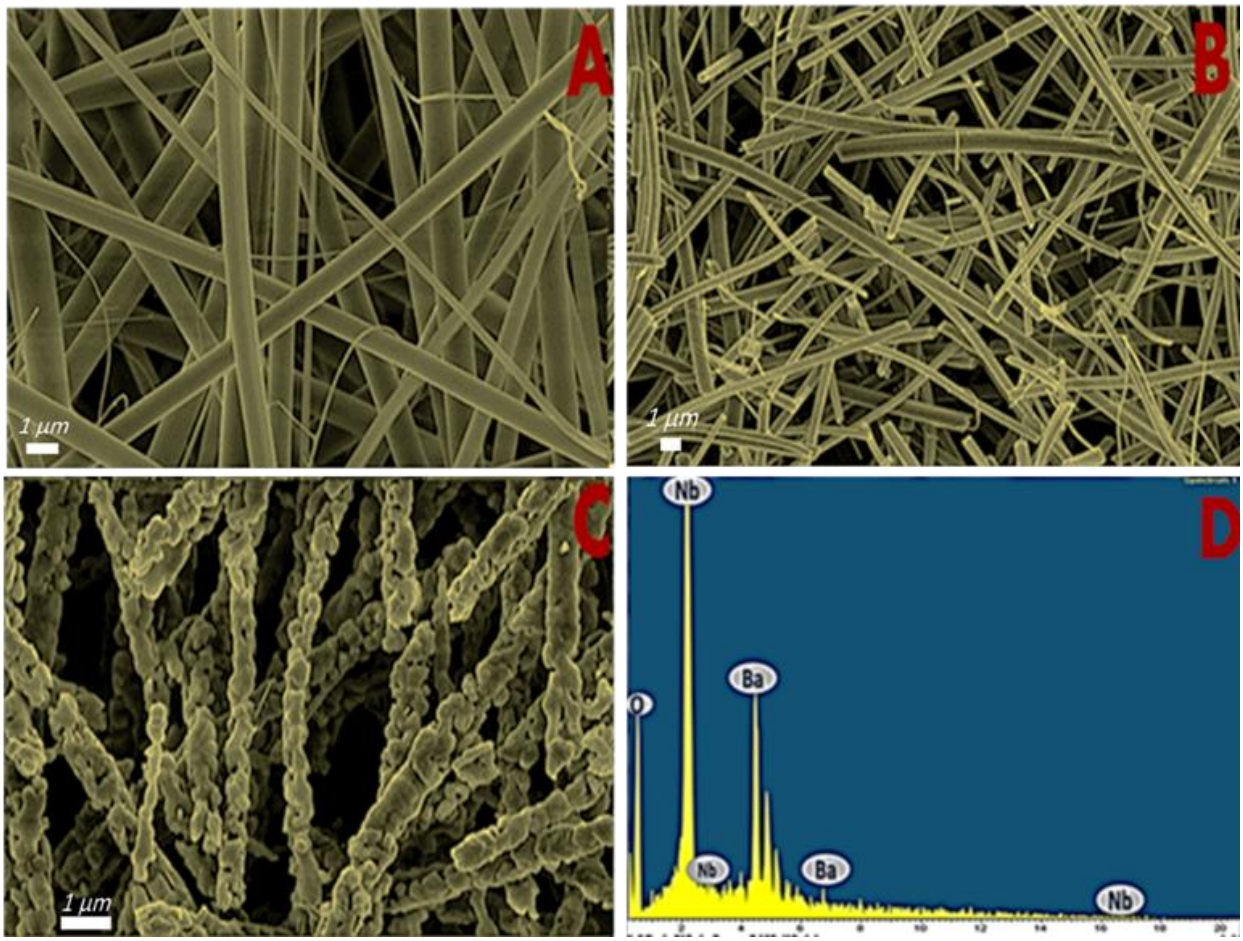

Figure 5-9 SEM images of $BaNb_2O_6$ nanofibers (A) as-synthesized, (B) after calcination at 650 ^oC, and (C) after calcination at 950 ^oC; along with (D) the corresponding EDX analysis.

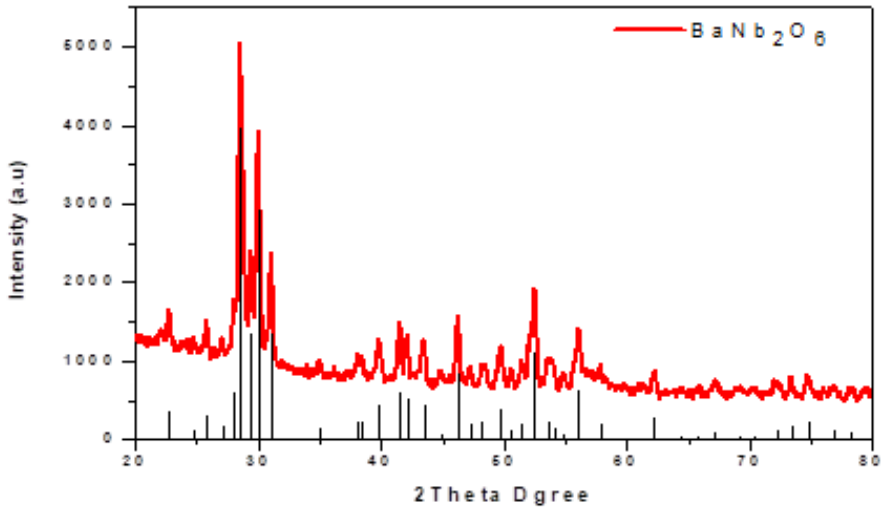

Figure 5-10 PXRD patterns of $BaNb_2O_6$.

crystals lying over each other.

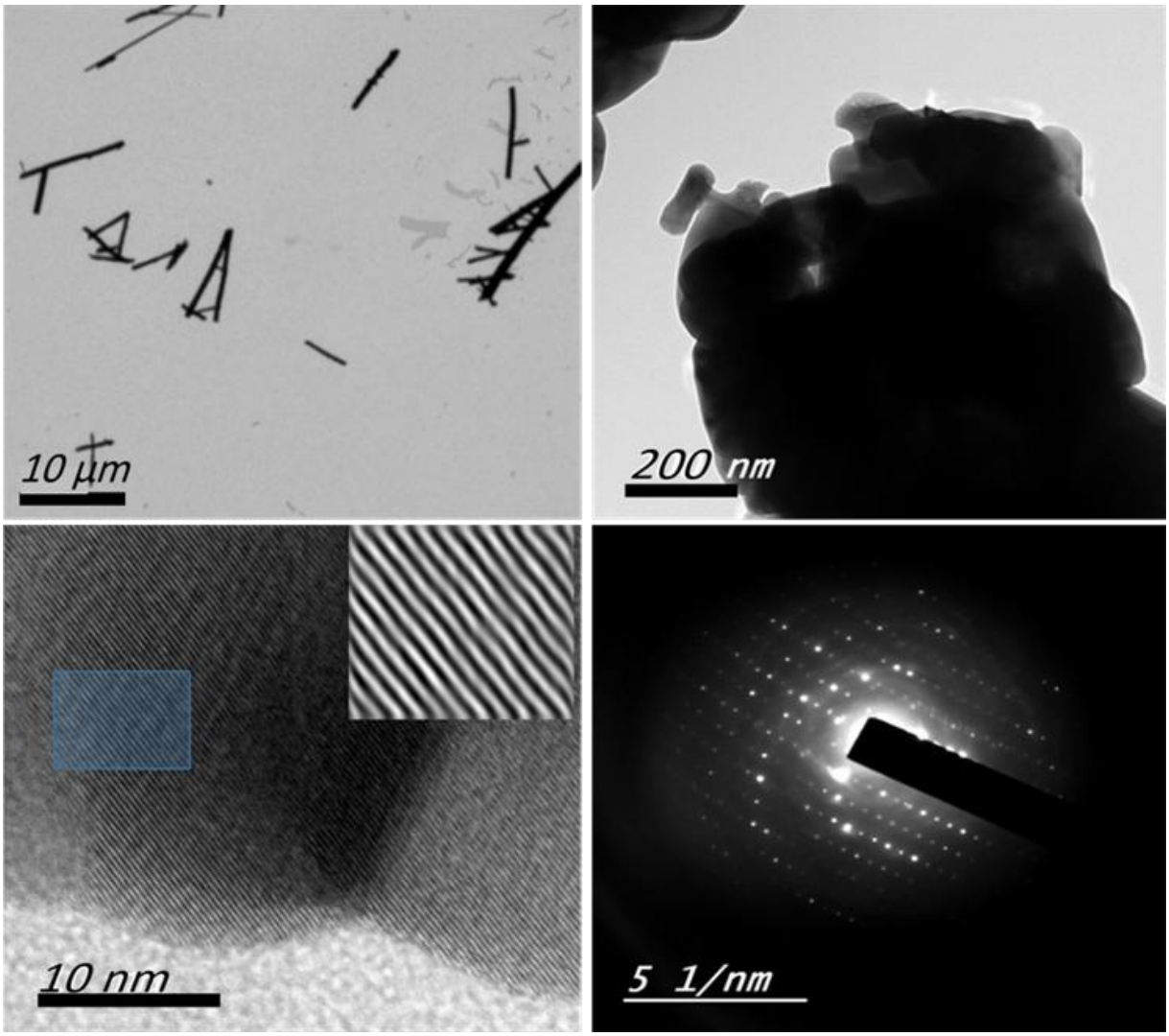

Figure 5-11 TEM images of the prepared $BaNb_2O_6$ nanofibers after calcination at 950 °C. SAED pattern shows the high crystallinity of the nanofibers.

5.2.2 Electrochemical Behavior of LOR at Different Electrodes

To confirm that $BaNb_2O_6$/CPE has no electroactivity within the designated potential range, initial assessment was carried out in the absence of LOR, in which neither anodic nor cathodic measurable peak currents were detected. On the other hand, CVs of both bare and modified CPEs were examined for the electrochemical sensing of LOR, Figure 5-12A. Electrochemical oxidation of LOR showed anodic current peak, which increased in the presence of nano-perovskite fiber as a CPE

modifier compared to the unmodified CPE counterpart. Note that the anodic peak current (I_p) was significantly improved in the presence of $BaNb_2O_6$ perovskite. This increase can be related to the ease of electron transfer kinetics as a result of the

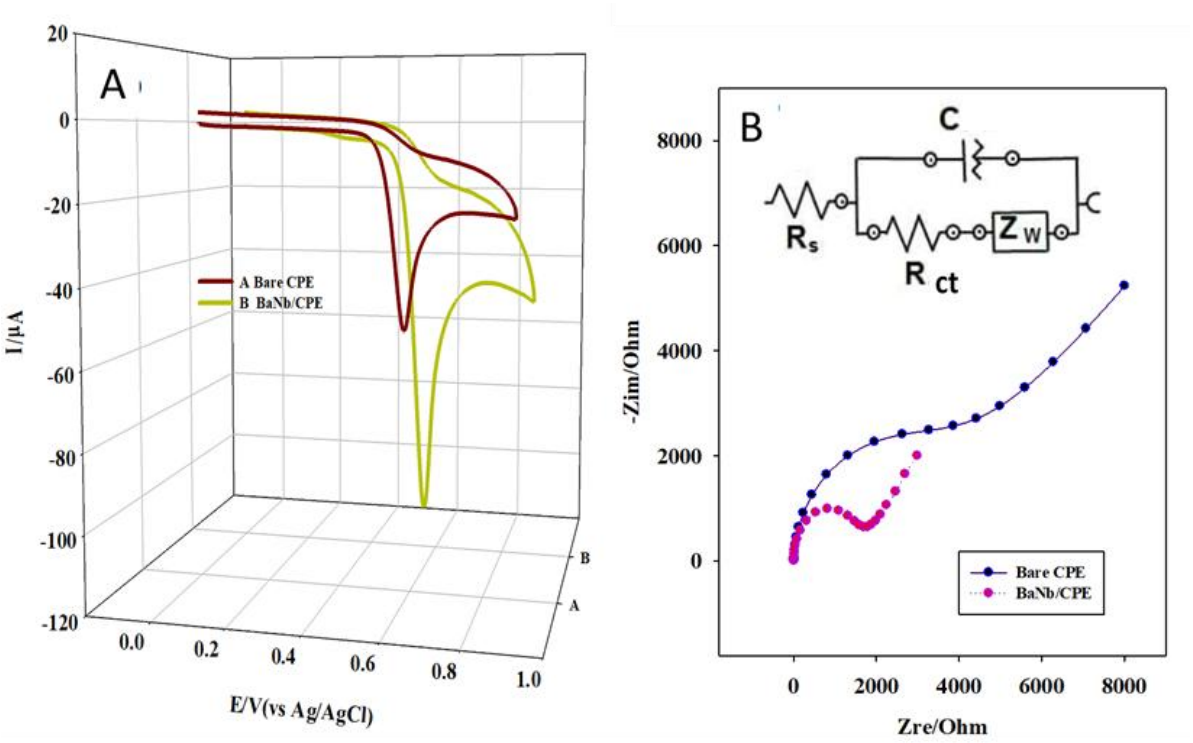

Figure 5-9 (A) Cyclic voltammograms of 1.0 x 10^{-4} M LOR in B–R buffer pH 7.0, at a scan rate of 100 mV s^{-1}, recorded at CPE and $BaNb_2O_6$/CPE electrodes. (B) EIS plots for both CPE and $BaNb_2O_6$/CPE in 5.0 x 10^{-3} M $[Fe(CN)_6]^{3-/4-}$ (1:1) solution in 0.1 M KCl.

catalytic properties of $BaNb_2O_6$ perovskite, which enjoys high surface area.

To get insights into the kinetics, mass-transport, and charge transfer coefficient of the new modified CPE, EIS measurements were performed in 5.0 mM $K_3Fe(CN)_6$ (1:1) solution in 0.1 M KCl, Figure 5-12B. The EIS plots showed both semicircular and linear part. In the high frequency region, the diameter of the verified semicircle corresponds to the charge transfer resistance (R_{ct}) across the electrode-electrolyte interface. Therefore, a general qualitative analysis of the observed Nyquist plots would suggest that the diminution of the semi-circle diameter for the $BaNb_2O_6$-modified CPE indicates an enhanced charge transfer, as juxtaposed with the

unmodified CPE. The inset of Figure 5-12B shows the correspondent circuit model used to fit the resultant impedance data; where R_{ct} is the charge transfer resistance, Z_W is the Warburg-type impedance (governing the diffusion process), and C is the interfacial capacitance. From the fitted data, R_{CT} was 3909.12 Ω at the bare CPE, whereas it slumped to 1401.78 Ω for $BaNb_2O_6$/CPE, manifesting the enhanced electron transfer on the $BaNb_2O_6$/CPE surface. These findings are in good agreement with the CV results, suggesting that the $BaNb_2O_6$/CPE composite would grant more electrically conductive pathways owing to the synergistic influence of its components.

5.2.3 Optimization of the Experimental Conditions

5.2.3.1 Influence of pH

As solution pH is an important variable affecting the resulted current magnitude and voltammogram shape, its influence was investigated upon the electro-oxidation of LOR with ASSWV, Figure 5-13. The peak potential shifts toward zero (less positive) as the pH goes higher (from 2.0 to 9.0), suggesting the contribution of a protonation-deprotonation process in the electrochemical oxidation of LOR.[27] Regarding the peak potential (E_p), the voltammetric measurements revealed a linear correspondence with the pH of the buffer solution as: $E_p(mV)$ = 680.20 - 29.97 pH; (R^2=0.9985). Moreover, the best fit line of the data follows the Nernstian behavior, signifying that this electrochemical process entails one proton and two electrons transfer reaction. The suggested mechanism of oxidation is illustrated in the Scheme 5-1. Note that raising the pH of the solution leads to an increase in the peak current, till it reaches a maximum at about pH 7.0, then it decreases. This is probably because at higher pH values the electrochemical reaction is more difficult due to the deficiency of protons. Consequently, pH 7.0 was selected for the rest of the experiments.

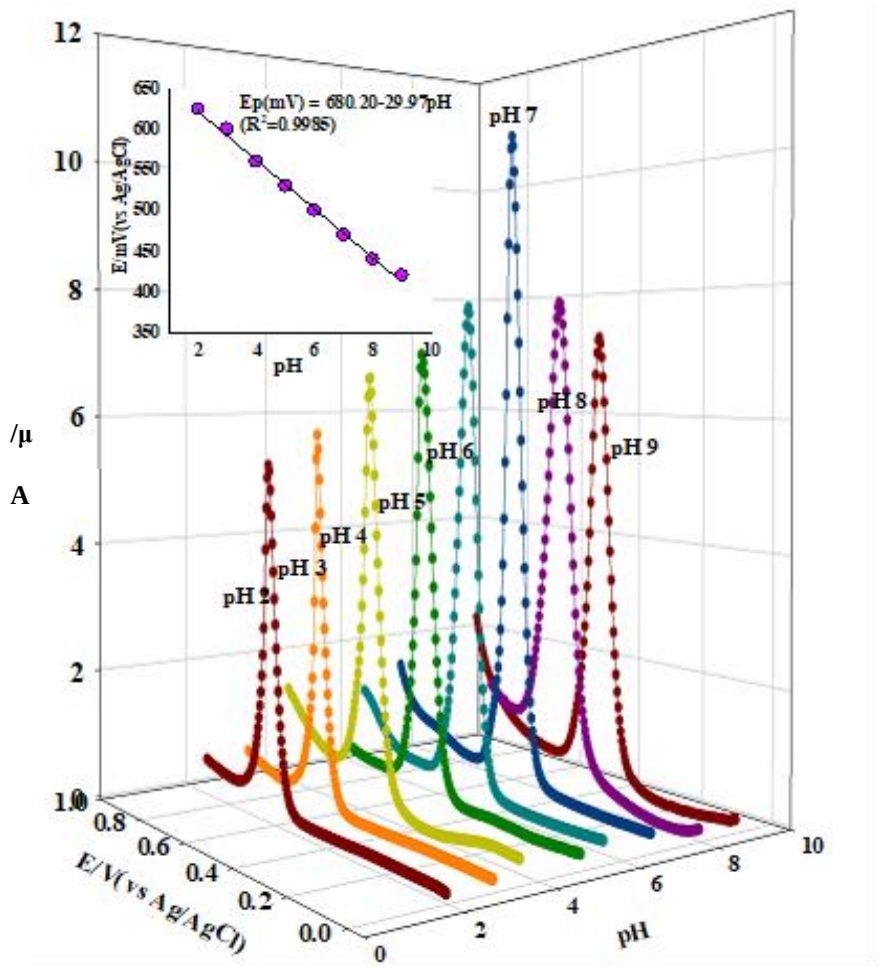

Figure 5-10 ASSWV response of $BaNb_2O_6$/CPE sensing platform, in a solution containing 1.0 x 10^{-4} M LOR at different pH values (in range 2.0 − 9.0); scan rate: 10 mV s^{-1}. The inset plots the LOR anodic peak potential vs. pH.

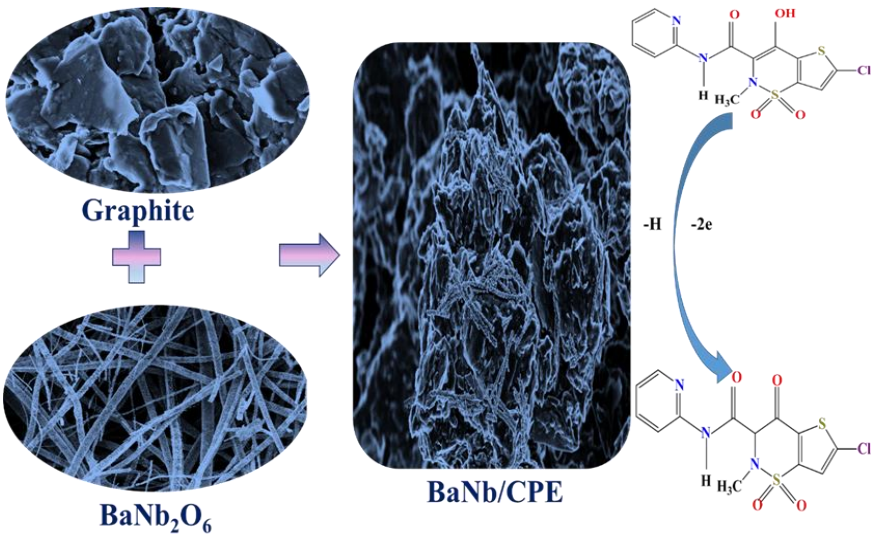

Scheme 5-2: Proposed mechanism of LOR detection on $BaNb_2O_6$ surface.

5.2.3.2 Effect of Scan Rate

The effect of scan rate (v), ranging from 10 − 100 mV s^{-1}, in B-R buffer (pH 7), on the electrochemical response of 1.0 $\times 10^{-4}$ M LOR on $BaNb_2O_6$/CPE was investigated to understand more about the electrode reaction mechanism, see Figure 5-14. As shown in inset A of Figure 5-14, a linear relationship was obtained between the peak current (I_{pa}) and $v^{1/2}$, indicating that the process is likely to be diffusion-controlled. The equivalent equation is: $I_p(\mu A) = -36.80 + 13.39\ v^{1/2}\ (V\ s^{-1})^{1/2}$, with a regression coefficient of 0.9975. Furthermore, it was observed that the oxidation peak potential (E_p) is also a function of scan rate, where increasing the scan rate causes the potential to shift toward more positive values, inset B of Figure 5-14. The regression equation: y=48.89a+449.04, (R^2=0.9937) describes the linear relationship of E_p and log v.

5.2.4 Chronoamperometric Measurements

The chronoamperometric experiments of different concentrations of LOR are shown in Figure 5-15, where a constant DC potential of +570 mV vs. Ag/AgCl was applied on $BaNb_2O_6$ /CPE in 0.04 M B-R buffer of pH 7.0. Inset A in the Figure 5-15 shows different current plots, sampled at constant time as a function of the concentration of LOR. For materials which are electroactive with a diffusion coefficient (D), the current analogous to their electrochemical reactions (under diffusion control) can be estimated by Cottrell's equation.[28] In the addressed measurements, with a time of 30 s, Cottrell current was found to increase by raising LOR concentration. Plotting I *vs.* $t^{-1/2}$ resulted in a straight line (inset 5-15A) whose slope (inset 5-15B) was used to obtain the value of D.[12] Accordingly, the diffusion coefficient was estimated to be 5.51×10^{-5} $cm^2\ s^{-1}$ for LOR.

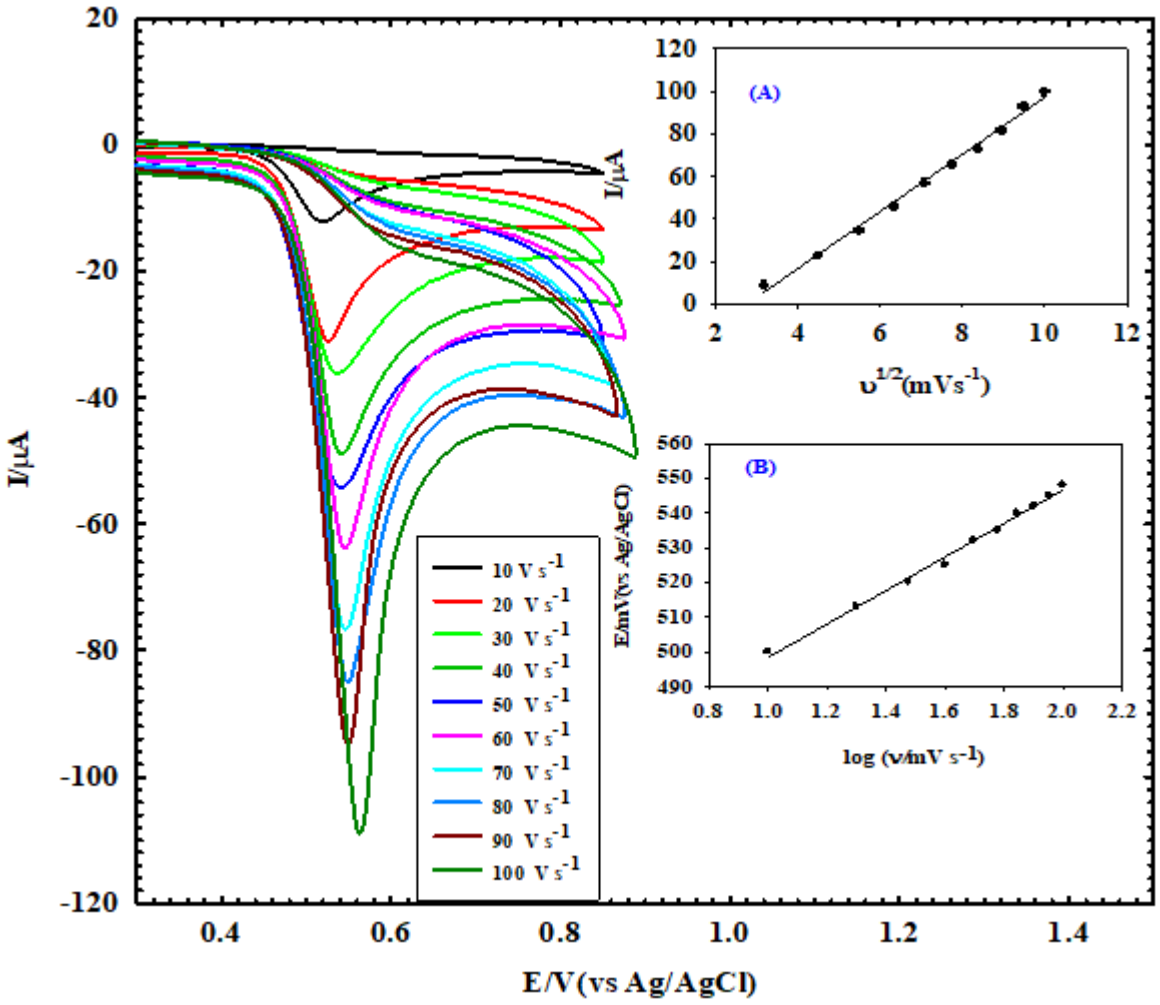

Figure 5-11 (A) Cyclic voltammograms of 1.0 $\times 10^{-3}$M LOR in B-R buffer (pH 7) using a $BaNb_2O_6$/CPE sensor at various scan rates: 10-100 mV.s^{-1}. Inset A: plot of I_p vs. $v^{1/2}$. Inset B: plot of Ep vs. log v.

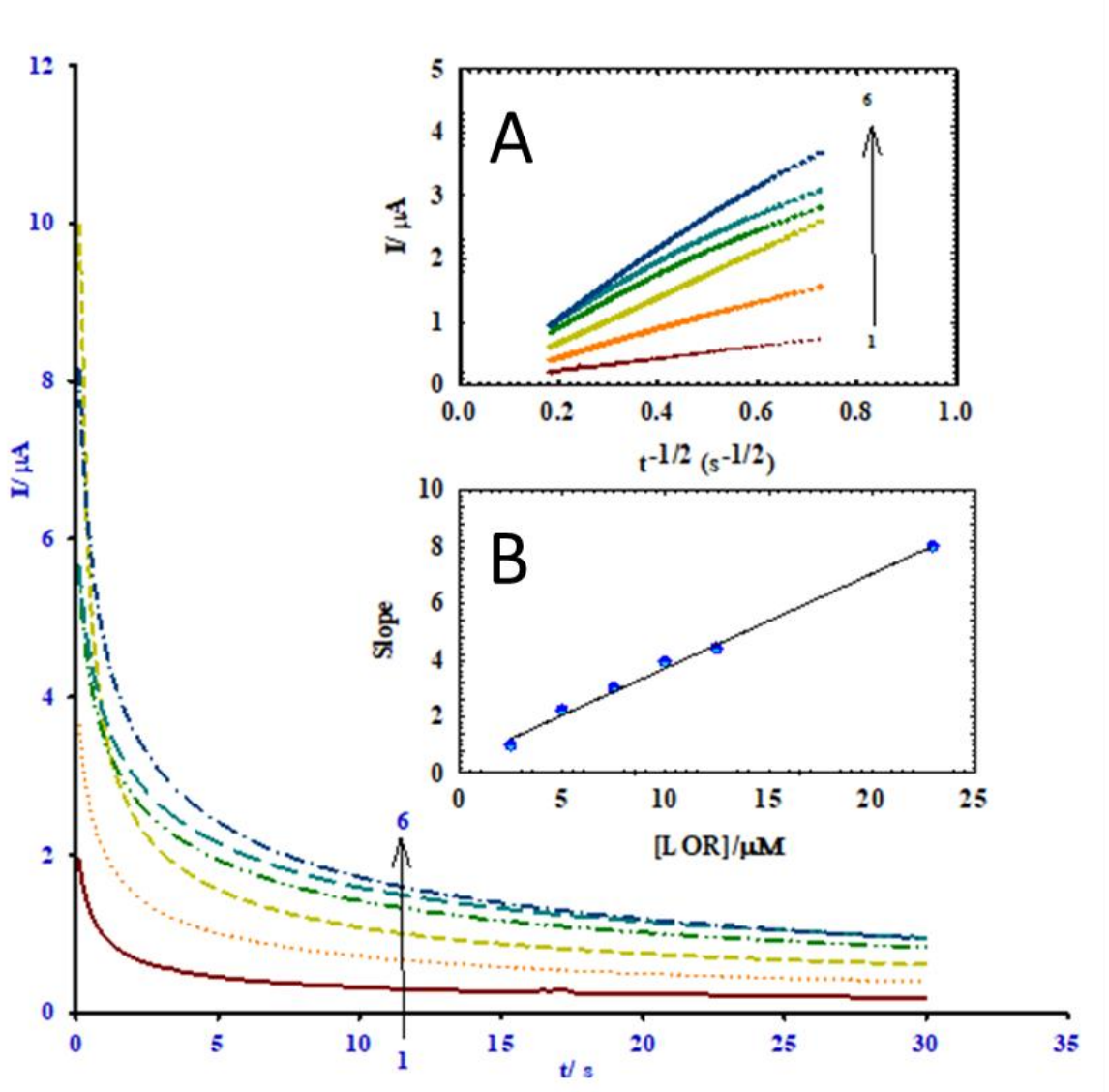

Figure 5-12. CA of different LOR concentrations at $BaNb_2O_6$/CPE surface in BR buffer (pH 7), for a potential step of +570 mV vs. Ag/AgCl. The numbers 1 to 6 in Cottrell's plot (inset A) correspond to 2.5, 5.0, 7.5, 10.0, 12.5, and 23.0 $x10^{-6}$ M of LOR, respectively.

5.2.5 Analytical Characterization and Method Validation

Design of experiments for optimization is a beneficial technique for extracting factors' effects on certain response.[29] As a common experimental technique, response surface methodology (RSM) was used for optimizing analytical procedures. RSM can estimate second order prediction formula along with interaction effects. However, it required substantial number of experiments in numerous factor designs. Therefore, factors should be limited in the first instance to apply RSM. Screening for influential

factors such as pH, nanofiber amount, scan rate, pulse height, pulse width along with accumulation potential and time was experimentally conducted beforehand. This study revealed that nanofibers amount, scan rate and accumulation time are substantially affecting the current. A face centered design was applied which is a special type of central composite design for RSM optimization. Figure 5-16 shows eight experiments at the vertices of the cube, six experiments on face axial points (i.e. axial value =1), and a center point repeated 2 times in order to improve the mathematical prediction model. Ball markers, in the same Figure, are scaled relative to the magnitude of measured current for each experiment.

The mathematical prediction model for current (I) was calculated from linear, quadratic and interaction terms as follow:

$$I = 4.69 - 0.50X_1 - 0.53X_1^2 + 0.40X_2 - 0.034X_2^2 - 0.20X_3 - 0.034X_3^2 - 0.25X_1X_2 + 0.25X_1X_3 + 1.5X_2X_3$$

where $X_1, X_2,$ and X_3 were composite amount, scan rate and deposition time, respectively.

Comparing coefficients of main effects, we can conclude that amount of composite has the largest negative effect and hence response would be maximized at low level of this factor, Figure 5-17A. However, its relatively large quadratic term would noticeably decrease the current at either extreme levels, Figure 5-17B. Therefore, optimum amount of composite would lay between maximum and minimum levels. Other main effects are affecting the response insignificantly, but high level of scan rate and low level of accumulation time are favorable to design's target. In addition, their corresponding quadratic terms are too trivial to exhibit curvatures in their response function and therefore insignificant. Interactions were

registered in the prediction model as well, Figure 5-17C. As the largest value of interaction coefficient, scan rate and deposition time interaction term (X_2X_3) is statistically significant (p=0.0125). Figure 5-17D shows that current is increased where the two factors are simultaneously at their maximum or minimum levels. Current is decreased at center points of both whereas sharp decrease in response is observed at low level of scan rate and high level of deposition time. Contrary to foregoing assessment of deposition time based on its main effect, the significant interaction necessitates applying high level of this factor along with scan rate which would dramatically increase response. Final optimization suggested using 10 mg% composite along with scan rate of 40 mV s^{-1} and accumulation time 180 s that would maximize the obtained current.

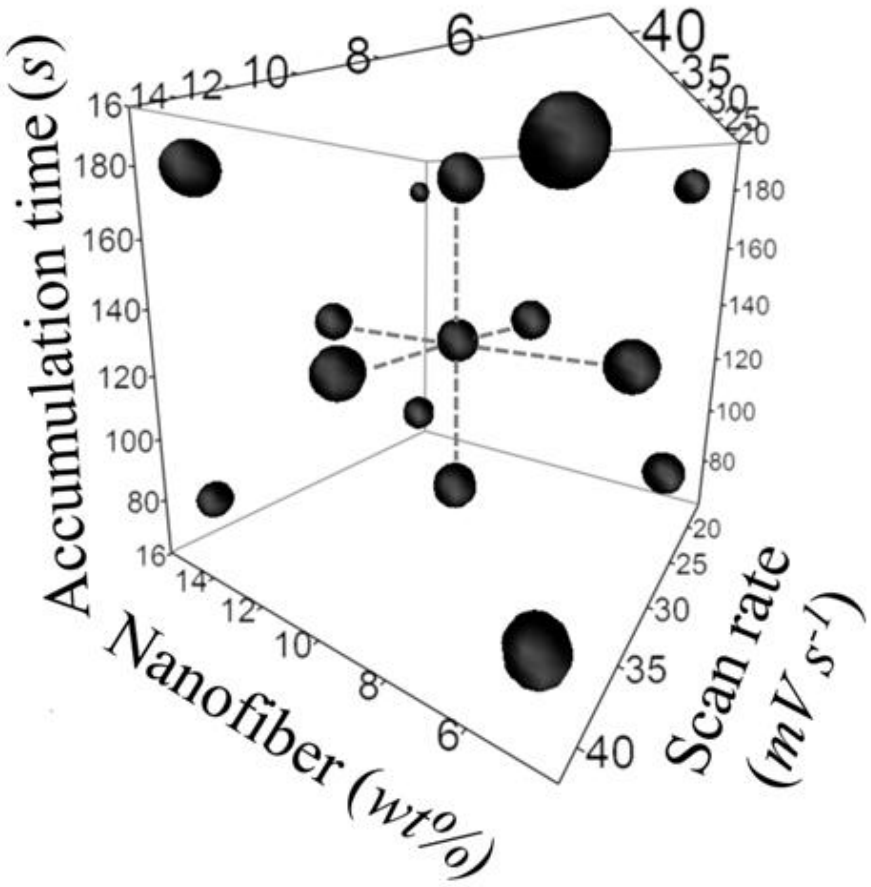

Figure 5-13 3D scatter plot of face centered design on three factors and current as a response; size of ball markers is relevant to measures current.

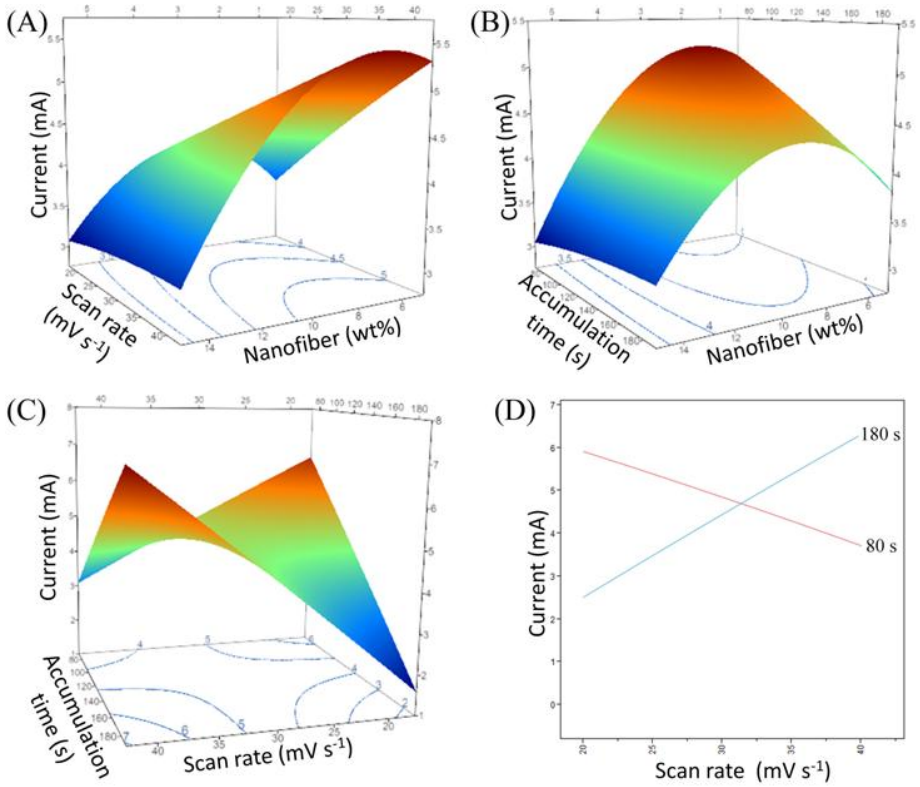

Figure 5-14 Surface plots of factors effects on current (A, B, and C) Interaction plot for current showing effect of scan rate at maximum and minimum levels of deposition time.

5.2.6 Stripping Behavior Towards LOR

The methods used to validate our proposed sensing platform were designed according to the protocols instructed by the International Conference on Harmonization (ICH) for methods validation.[30] SWASV measurements were carried out using $BaNb_2O_6$/CPE in solutions of different concentrations of LOR, in the presence of B-R buffer pH 7.0. The range of calibration was designed to take the essential practical range into consideration, according to the concentration range of LOR in the common pharmaceutical drugs, providing linear and precise results. Figure 5-18 shows the results of plotting the peak current *vs.* LOR concentration, in which two linear ranges, with different slopes, of LOR concentrations were obtained.

For the range 4.0×10^{-9}– 1.0×10^{-6} M, the regression equation was I(μA) = 0.101 C + 0.012 (R^2 = 0.9994), while for 1.0×10^{-6} – 2.5×10^{-4} M, the regression equation was I(μA) = 0.088 C + 0.763 (R^2 = 0.9992). The lower slope (indicating sensitivity) of the second linear range can be attributed to kinetic limitations.[31]

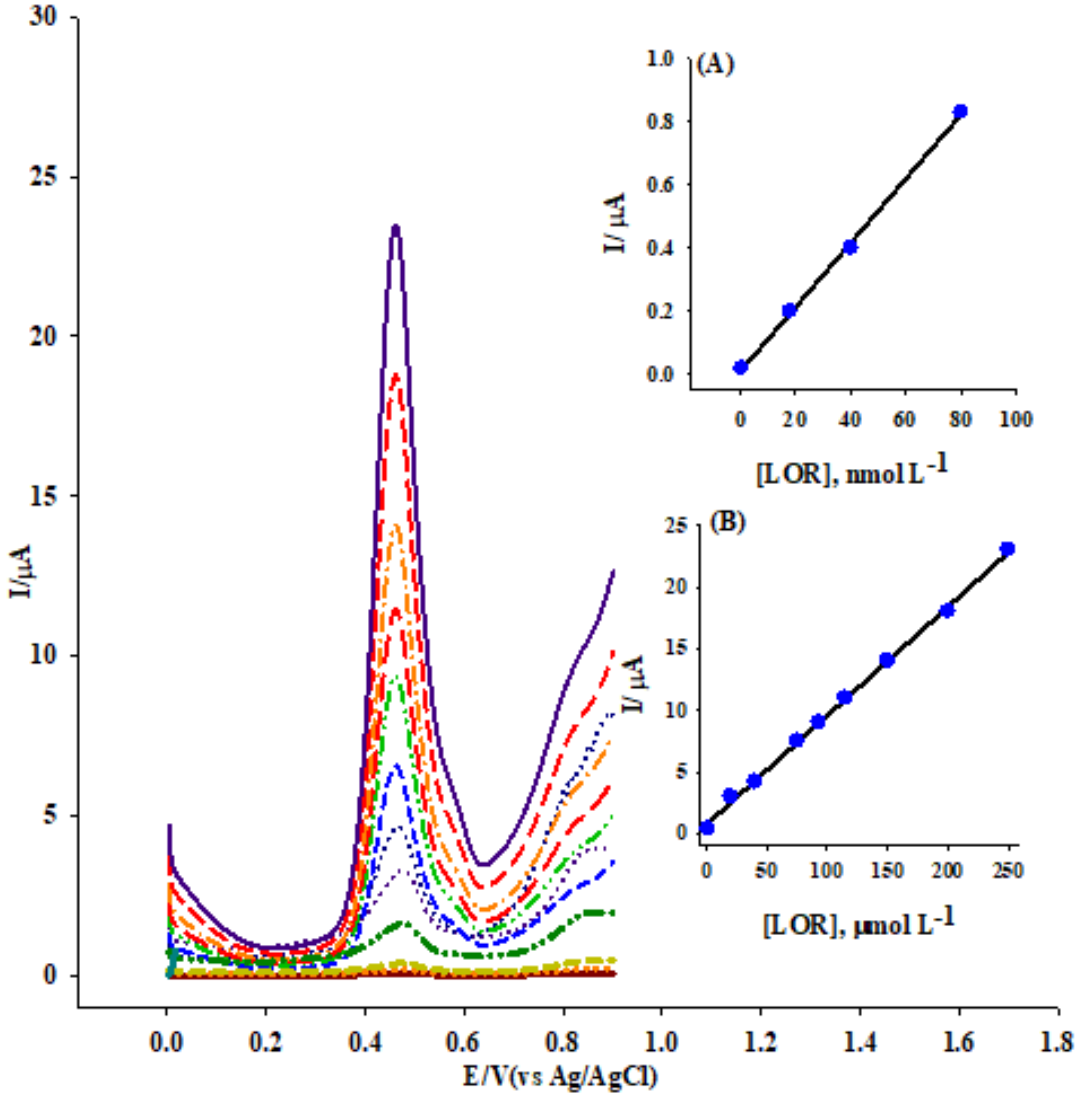

Figure 5-15 ASSWV at $BaNb_2O_6$/CPE in solutions containing different concentrations of LOR, using B–R buffer (pH 7.0), at a scan rate of 40 mV s^{-1}. Insets: the plot of the peak current as a function of LOR in concentration range 4.0×10^{-9} – 1.0×10^{-6} M (A), and 1.0×10^{-6} – 2.5×10^{-4} M (B).

LOD was found to be 6.39×10^{-10} M, which was calculated from the equation LOD = *3S/x*; where *S* is the standard deviation of 5 repetitive results of the oxidation

peak current, and *x* is the slope of the resulted calibration curve. Also, the LOQ was calculated to be 2.13×10^{9} M, using the equation LOQ = *10S/x*; where *S* is the standard deviation of the intercept and *x* is the slope of the regression line. The intra-day (within-day) and inter-day (between-day) precisions ranged in 0.74–1.19% and 0.65–1.24%, respectively. The stability of the modified electrode has been studied, where over 10 days of storage in air, the peak current response has recorded almost the same value. Moreover, the proposed electrode has maintained 98.12% of its first response over a period of one month.

5.2.7 Selective Determinations of LOR and PAR

The selective and sensitive detection of LOR and PAR in their co-formulated mixtures was performed using ASSWV technique. In the LOR and PAR mixtures, the concentration of one drug was to be changed while keeping the other constant and vice versa, Figure 5-19A. The peak current of LOR showed a positive proportionality with its concentration in the range of $1.12 \times 10^{-6} – 2.50 \times 10^{-4}$ M, whereas the current of PAR was almost the same at 3.30×10^{-4} M. Likewise, at a constant concentration of LOR, the current response of PAR was changing in correspondence to its concentration, Figure 5-19B. Note that PAR current peaks vary linearly over the concentration range of $5.00 \times 10^{-7} – 1.00 \times 10^{-3}$ M, with the LOR concentration constant at 1.20×10^{-6} M.

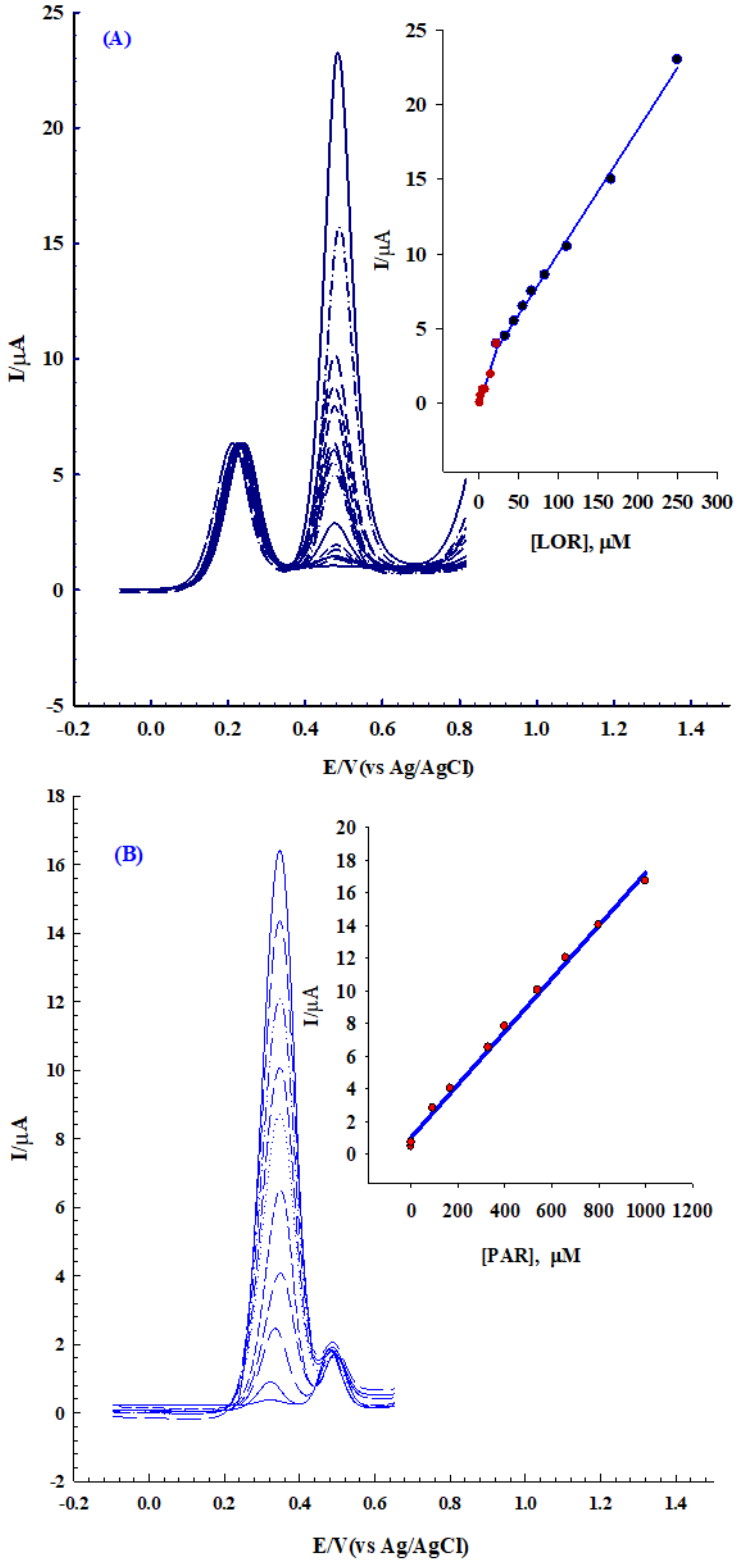

Figure 5-16 (A) ASSWV at $BaNb_2O_6$/CPE in B-R buffer of pH 7.0 of 1.12 x 10^{-6}–2.50 x 10^{-4} M LOR at fixed concentration of 3.30 x 10^{-4} M PAR; Inset: the plot of the peak current as a function of LOR concentration. (B) ASSWV at $BaNb_2O_6$/CPE in B-R buffer of pH 7.0 of 5.00 x 10-7 –1.00 x 10-3 M PAR at fixed concentration of LOR 1.20 x 10-6 M and their corresponding calibration curves; Inset: the plot of the peak current as a function of PAR concentration.

5.2.8 Analysis of Spiked Plasma Samples

The applicability of $BaNb_2O_6$/CPE to determinate both LOR and PAR in human plasma was examined. Using the standard addition method, concentrations were detected by applying the calibration curve, with the results presented in Table 5-3. The recovery percentages show a good precision of the suggested sensor. The experimental results show that the proposed sensor has excessive potential for the simultaneous trace-level detection of LOR and PAR in biological fluids.

Table 5-3. Determination of LOR and PAR concentrations in human plasma samples.

Sample	Amount added standard (µM)	Amount found* (µM)	Apparent recovery%
LOR	20.00	20.10±0.32	100.50
	40.00	39.97±0.56	99.92
	60.00	58.98±097	98.30
	80.00	80.12±1.18	100.15
	100.00	98.87±2.07	98.87
Recovery%±R.S.D			99.55±0.93
PAR	20.00	20.05±0.16	100.25
	40.00	40.13±0.30	100.32
	60.00	59.87±0.42	99.78
	80.00	80.21±0.91	100.26
	100.00	99.43±1.02	99.43
Recovery%±R.S.D			100.02±0.39

*Based on three experimental measurements.

5.3 References

(1) Deng, S.; Berry, V. Wrinkled, Rippled and Crumpled Graphene: An Overview of Formation Mechanism, Electronic Properties, and Applications. *Mater. Today* **2016**, *19* (4), 197–212.

(2) Acik, M.; Lee, G.; Mattevi, C.; Chhowalla, M.; Cho, K.; Chabal, Y. J. Unusual Infrared-Absorption Mechanism in Thermally Reduced Graphene Oxide. *Nat. Mater.* **2010**, *9* (10), 840–845.

(3) Zhang, H.; Lv, X.; Li, Y.; Wang, Y.; Li, J. P25-Graphene Composite as a High Performance Photocatalyst. *ACS Nano* **2009**, *4* (1), 380–386.

(4) Liang, D.; Cui, C.; Hu, H.; Wang, Y.; Xu, S.; Ying, B.; Li, P.; Lu, B.; Shen, H. One-Step Hydrothermal Synthesis of Anatase TiO_2/Reduced Graphene Oxide Nanocomposites with Enhanced Photocatalytic Activity. *J. Alloys Compd.* **2014**, *582*, 236–240.

(5) Wang, J.; Wang, M.; Xiong, J.; Lu, C. Enhanced Photocatalytic Activity of a TiO_2/Graphene Composite by Improving the Reduction Degree of Graphene. *New Carbon Mater.* **2015**, *30* (4), 357–363.

(6) Tan, L.-L.; Ong, W.-J.; Chai, S.-P.; Mohamed, A. R. Reduced Graphene Oxide-TiO_2 Nanocomposite as a Promising Visible-Light-Active Photocatalyst for the Conversion of Carbon Dioxide. *Nanoscale Res. Lett.* **2013**, *8* (1), 465.

(7) Marcano, D. C.; Kosynkin, D. V; Berlin, J. M.; Sinitskii, A.; Sun, Z.; Slesarev, A.; Alemany, L. B.; Lu, W.; Tour, J. M. Improved Synthesis of Graphene Oxide. **2010**.

(8) Fan, W.; Lai, Q.; Zhang, Q.; Wang, Y. Nanocomposites of TiO_2 and Reduced

Graphene Oxide as Efficient Photocatalysts for Hydrogen Evolution. *J. Phys. Chem. C* **2011**, *115* (21), 10694–10701.

(9) Cullity, B. D.; Weymouth, J. W. Elements of X-Ray Diffraction. *Am. J. Phys.* **1957**, *25* (6), 394–395.

(10) Zhou, Y.; Bao, Q.; Tang, L. A. L.; Zhong, Y.; Loh, K. P. Hydrothermal Dehydration for the "Green" Reduction of Exfoliated Graphene Oxide to Graphene and Demonstration of Tunable Optical Limiting Properties. *Chem. Mater.* **2009**, *21* (13), 2950–2956.

(11) Perera, S. D.; Mariano, R. G.; Vu, K.; Nour, N.; Seitz, O.; Chabal, Y.; Balkus Jr, K. J. Hydrothermal Synthesis of Graphene-TiO_2 Nanotube Composites with Enhanced Photocatalytic Activity. *Acs Catal.* **2012**, *2* (6), 949–956.

(12) Compton, R. G.; Banks, C. E. *Understanding Voltammetry*; World Scientific, 2011.

(13) Samir, M.; Salama, M.; Allam, N. K. Sub-100 Nm TiO_2 Tubular Architectures for Efficient Solar Energy Conversion. *J. Mater. Chem. A* **2016**, *4* (24), 9375–9380.

(14) Wei, Y.; Gao, C.; Meng, F.-L.; Li, H.-H.; Wang, L.; Liu, J.-H.; Huang, X.-J. SnO_2/Reduced Graphene Oxide Nanocomposite for the Simultaneous Electrochemical Detection of Cadmium (II), Lead (II), Copper (II), and Mercury (II): An Interesting Favorable Mutual Interference. *J. Phys. Chem. C* **2011**, *116* (1), 1034–1041.

(15) Bagheri, H.; Afkhami, A.; Khoshsafar, H.; Rezaei, M.; Sabounchei, S. J.; Sarlakifar, M. Simultaneous Electrochemical Sensing of Thallium, Lead and

Mercury Using a Novel Ionic Liquid/Graphene Modified Electrode. *Anal. Chim. Acta* **2015**, *870*, 56–66.

(16) Fan, Y.; Lu, H.-T.; Liu, J.-H.; Yang, C.-P.; Jing, Q.-S.; Zhang, Y.-X.; Yang, X.-K.; Huang, K.-J. Hydrothermal Preparation and Electrochemical Sensing Properties of TiO_2–graphene Nanocomposite. *Colloids Surfaces B Biointerfaces* **2011**, *83* (1), 78–82.

(17) Wang, X.; Li, G.; Liu, L.; Cheng, Y.; Zheng, W.; Wu, S.; Wu, F.; Sun, W. Application of Titanium Dioxide Nanowires and Electroreduced Graphene Oxide Modified Electrodes for the Electrochemical Detection of Specific Tlh Gene Sequence from Vibrio Parahaemolyticus. *Anal. Methods* **2015**, *7* (6), 2623–2629.

(18) Amiri, M.; Salehniya, H.; Habibi-Yangjeh, A. Graphitic Carbon Nitride/Chitosan Composite for Adsorption and Electrochemical Determination of Mercury in Real Samples. *Ind. Eng. Chem. Res.* **2016**, *55* (29), 8114–8122.

(19) Bhanjana, G.; Dilbaghi, N.; Bhalla, V.; Kim, K.-H.; Kumar, S. Direct Ultrasensitive Redox Sensing of Mercury Using a Nanogold Platform. *J. Mol. Liq.* **2017**, *225*, 598–605.

(20) Chen, L.; Chen, Z.-N. A Multifunctional Label-Free Electrochemical Impedance Biosensor for Hg^{2+} , Adenosine Triphosphate and Thrombin. *Talanta* **2015**, *132*, 664–668.

(21) Duarte, K.; Justino, C. I. L.; Freitas, A. C.; Gomes, A. M. P.; Duarte, A. C.; Rocha-Santos, T. A. P. Disposable Sensors for Environmental Monitoring of Lead, Cadmium and Mercury. *TrAC Trends Anal. Chem.* **2015**, *64*, 183–190.

(22) Zhang, Y.; Zhao, H.; Wu, Z.; Xue, Y.; Zhang, X.; He, Y.; Li, X.; Yuan, Z. A Novel Graphene-DNA Biosensor for Selective Detection of Mercury Ions. *Biosens. Bioelectron.* **2013**, *48*, 180–187.

(23) Wei, J.; Yang, D.; Chen, H.; Gao, Y.; Li, H. Stripping Voltammetric Determination of Mercury (II) Based on SWCNT-PhSH Modified Gold Electrode. *Sensors Actuators B Chem.* **2014**, *190*, 968–974.

(24) Ameen, S.; Akhtar, M. S.; Seo, H.-K.; Shin, H.-S. TiO_2 Nanotube Arrays via Electrochemical Anodic Oxidation: Prospective Electrode for Sensing Phenyl Hydrazine. *Appl. Phys. Lett.* **2013**, *103* (6), 61602.

(25) Abdellah, A. M.; Hafez, A.; Panikkanvalappil, S. R.; El-Sayed, M. A.; Allam, N. K. Single-Crystal Electrospun Plasmonic Perovskite Nanofibers. *J. Phys. Chem. C* **2018**, *122*, 27.

(26) Hildebrandt, N. C.; Soldat, J.; Marschall, R. Layered Perovskite Nanofibers via Electrospinning for Overall Water Splitting. *Small* **2015**, *11* (17), 2051–2057.

(27) Huang, L.; Bu, L.; Zhao, F.; Zeng, B. Voltammetric Behavior of Ethopropazine and the Influence of Sodium Dodecylsulfate on Its Accumulation on Gold Electrodes. *J. Solid State Electrochem.* **2004**, *8* (12), 976–981.

(28) Bard, A. J.; Faulkner, L. R.; Leddy, J.; Zoski, C. G. Electrochemical Methods: Fundamentals and Applications (Vol. 2): Wiley New York. **1980**.

(29) Mohamed, M. A.; Atty, S. A.; Yehia, A. M.; Foster, C. W.; Banks, C. E.; Allam, N. K. Electrochemical Determination of the Serotonin Reuptake Inhibitor, Dapoxetine, Using Cesium–Gold Nanoparticles. *ACS Omega* **2017**, *2* (10), 6628–6635.

(30) Guideline, I. C. H. H. T. Validation of Analytical Procedures: Text and Methodology. *Q2* **2005**, *1*.

(31) K Gupta, V.; Nayak, A.; Agarwal, S.; Singhal, B. Recent Advances on Potentiometric Membrane Sensors for Pharmaceutical Analysis. *Comb. Chem. High Throughput Screen.* **2011**, *14* (4), 284–302.

Chapter 6

Conclusion and Future Work[‡]

Market study of sensors is evident that more money will be invested in sensors industry as they have a real chance of progress during the following decades. The feasibility of developing their recognition ability makes electrochemical sensors a good candidate for application in many disciplines such as food, biomedical, environmental, agricultural, and industrial fields. To enhance the sensitivity of the electrochemical electrodes used, two novel nanostructures have been fabricated for environmental and pharmaceutical purposes.

The fist is TNT/RGO for improved detection of Hg(II) trace concentrations. The sensor exhibited low LOD, wide linear range, high selectivity, and good reusability. The fabricated electrode modifier displayed an efficient sensibility of Hg(II) in the presence of Cu(II) and Mn(II) species with no significant interference for a wide range of concentrations. The sensing platform also proved to be applicable for real sample analysis with very satisfactory results.

The second is $BaNb_2O_6$ nanofibers for enhanced determination of LOR low concentrations. The fabricated $BaNb_2O_6$/CPE sensor showed an enhanced activity towards the electrocatalytic oxidation of LOR and PAR, producing remarkably high oxidation currents. Wide linear dynamic ranges, high sensitivity, very low LOD, good

[‡] Parts of this chapter were published in Abdullah, Ibrahim H., Nashaat Ahmed, Mona A. Mohamed, Fawzy MA Ragab, Marwa TA Abdel-Wareth, and Nageh K. Allam. "An engineered nanocomposite for sensitive and selective detection of mercury in environmental water samples." *Analytical Methods* 10, no. 21 (2018): 2526-2535.

And in Mohamed, Mona A., Menna M. Hasan, Ibrahim H. Abdullah, Ahmed M. Abdellah, Ali M. Yehia, Nashaat Ahmed, Walaa Abbas, and Nageh K. Allam. "Smart bi-metallic perovskite nanofibers as selective and reusable sensors of nano-level concentrations of non-steroidal anti-inflammatory drugs." *Talanta* 185 (2018): 344-351.

reproducibility and repeatability, and high stability, together with simple procedures for surface modification and determination are the advantages of the prepared sensor.

It is supposed that as an extension for this thesis work, future research can be focused on:

1- Testing the TNT/RGO modifier in a photoelectrochemical cell for sensing purposes.

2- Testing $BaNb_2O_6$ modifier against other drugs of a chemical structure similar to that of LOR and PAR.

3- Trying to deposit both modifiers on SPE to get closer to a commercial model of sensors.

Publications

Abdullah, Ibrahim H., Nashaat Ahmed, Mona A. Mohamed, Fawzy MA Ragab, Marwa TA Abdel-Wareth, and Nageh K. Allam. "An engineered nanocomposite for sensitive and selective detection of mercury in environmental water samples." *Analytical Methods* 10, no. 21 (2018): 2526-2535.

Mohamed, Mona A., Menna M. Hasan, Ibrahim H. Abdullah, Ahmed M. Abdellah, Ali M. Yehia, Nashaat Ahmed, Walaa Abbas, and Nageh K. Allam. "Smart bi-metallic perovskite nanofibers as selective and reusable sensors of nano-level concentrations of non-steroidal anti-inflammatory drugs." *Talanta* 185 (2018): 344-351.